ISSN Application ID:13041

EP Journal of Heat and Mass Transfer

Volume No. 8

Issue No. 1

January - April 2024

ENRICHED PUBLICATIONS PVT. LTD

S-9, IInd FLOOR, MLU POCKET,
MANISH ABHINAV PLAZA-II, ABOVE FEDERAL BANK,
PLOT NO-5, SECTOR-5, DWARKA, NEW DELHI, INDIA-110075,
PHONE: - + (91)-(11)-47026006

ISSN Application ID: ID:13041

EP Journal of Heat and Mass Transfer

Aims and Scope

EP Journal of Heat and Mass Transfer is a peer reviewed journal published by Enriched Publication and articles are selected primarily on heat and mass transfer such as heat transfer in phase change phenomenon, machinery and welding operations turbulence etc. This journal consist of research articles and theoretical articles are also accepted of this subject.

ISSN Application ID: ID:13041

EP Journal of Heat and Mass Transfer

(Volume No. 8, Issue No. 1, January - April 2024)

Contents

Energy Analysis and Parametric Study of Flat Pate Collector Area of a Solar Driven Water-Lithium Bromide Half Effect Vapour Absorption Refrigeration System for a Given Cooling Load

Abhishek Verma[1], AkhileshArora[2], R. S. Mishra[3]

[1]P.G. Student, Mechanical Engineering Department, Delhi Technological University, Bawana Road Delhi-110042
e-mail-abhishek.ret@gmail.com

[2]Assistant Professor, Mechanical Engineering Department, Delhi Technological University, Bawana Road Delhi-110042 e-mail-akhilesharora@dce.ac.in

[3]Professor and Head of Dept., Mechanical Engineering Department, Delhi Technological University, Bawana Road Delhi-110042
e-mail-rsmishra1651956@yahoo.co.in

ABSTRACT

In the modern times,Solar Cooling systems are becoming popular to reduce the carbon footprint of air conditioning. The need and importance of solar based cooling system can play a very prominent role in attenuating energy crisis by the use of solar energy. This paper presents the thermodynamic analysis and calculation of flat plate collector area of vapour absorption half effect cooling system using sun as source of energy.The cooling load is assumed to be 25 kW. The evaporator temperature is maintained constant at 7°C and condenser temperature is varied from 30°C and 46°C and generators temperatures are varied from 65 to 85 °C. For a given condenser temperature (say 38°C) there is an optimum generator temperature for which the total area flat plate collector is minimum. This optimum generator temperature comes out to be 80°C. This generator temperature gives the maximum COP which is obtained as 0.4158. For these values the Area of flat plate collector on High Pressure side (Ah) is 130 m^2.Area of flat plate collector on Low Pressure side (Al) is 154 m^2. Total Area of flat plate collector (A) is 284 m^2.

Keywords - ***Half Effect, Energy Analysis, Vapour Absorption Refrigeration, Water-Lithium bromide, Flat plate Collector. Solar Driven.***

1. INTRODUCTION

At present, the conventional resources of energy are being reduced every day, led to the researchers to identify the systems which use renewable sources of energy. The depletion of conventional sources of energy not only increasing the cost of energy production but also polluting the environment in a severe manner. The refrigeration and air conditioning systems have a major demand of the total energy consumption of the world. The harmful emissions of fossil fuels and chlorine based refrigerants used are responsible for the global warming and the ozone layer depletion. All these problems have led the scientists to develop a refrigeration system which uses renewable sources of energy. The energy of the sun may be harnessed to produce the refrigerating effect which reduces the dependency on high-grade energy and do not pollute the environment.

The primitive characteristic of the half-effect absorption cycle is the running capableness at lower temperatures compared to others. The name “half-effect” rising from the COP, which is almost half that of the single-effect cycle. It must be eminent that COP of the half-effect vapour absorption system is comparatively less as it discard more heat than the absorption cycle working on single-effect, it is approx..50%. However, it can be work with the relatively low temperature heat **origin.[1]**.

Gomri [2] simulated the operation of a half-effect absorption refrigeration system of 10 kW. The energy from the sun is utilized to run the flat plate collector, which are used as the source of heat generation for the vapour absorption refrigeration system. The system has two units, one unit is for the generation of heat which would be utilized to run the second unit i.e. the absorption cooling unit.

Adhikari et al. [3] examined and evaluated the practicability of a vapour absorption refrigeration unit work on solar Energy. The system was designed with the postulate of vapour absorption refrigeration cycle with Lithium Bromide as an absorbing medium and water as a refrigerant.5 kW cooling load for the office building is considered. The designed absorption refrigeration system has COP equitable to 0.77. It proved that the best performance in terms of COP would be succeeded when operated at low generator temperature and the low generator heat. Solar collector area to conduct system is 8 m^2. On the increase of mass flow rate of the refrigerant, the overall cooling effect increases, but the COP decreases. The absorption cooling system is an alternative to the conventional vapour compression system.

Arora et al. [4] carried out the analysis of exergy and energy of half effect lithium bromide water vapor absorption refrigeration system. The optimum intermediate pressure is evaluated to maximize the exergetic efficiency and COP under different conditions. The optimum pressure for both maximum COP and exergy is same. The calculation of optimum pressure involves the effect of high and low pressure temperatures of generator, evaporator, difference of high and low pressure of generator and evaporator, effectiveness of heat exchangers carrying strong and weak solution of Lithium bromide and water. The maximum COP obtained in the range of 0.415 to 0.438,and the value of maximum efficiency is varied from 6.96 to 13.74%.

This paper presents the thermodynamic analysis and calculation of flat plate collector area of vapour absorption half effect cooling system using sun as source of energy.

2. THERMODYNAMIC ANALYSIS OF HALF EFFECT SYSTEM

The half-effect water-lithium (H_2O-$LiBr_2$) bromide vapour absorption refrigeration system, consists of an condenser, evaporator, LP & HP generators, LP & HP absorbers, LP and HP solution heat exchangers, , solution pumps and solution and refrigerant throttle valves. The condenser and HP generator work at same pressure which is the maximum pressure of the system. The LP generator and HP absorber work at the same intermediate pressure whereas the evaporator and the LP absorber work at same lowermost pressure of the system.

The refrigerant (i.e., water) is circulated through the condenser, evaporator, LP absorber, LP generator, HP absorber, HP generator. When the water vapour has condensed in the condenser, it revert to the evaporator through an expansion valve.

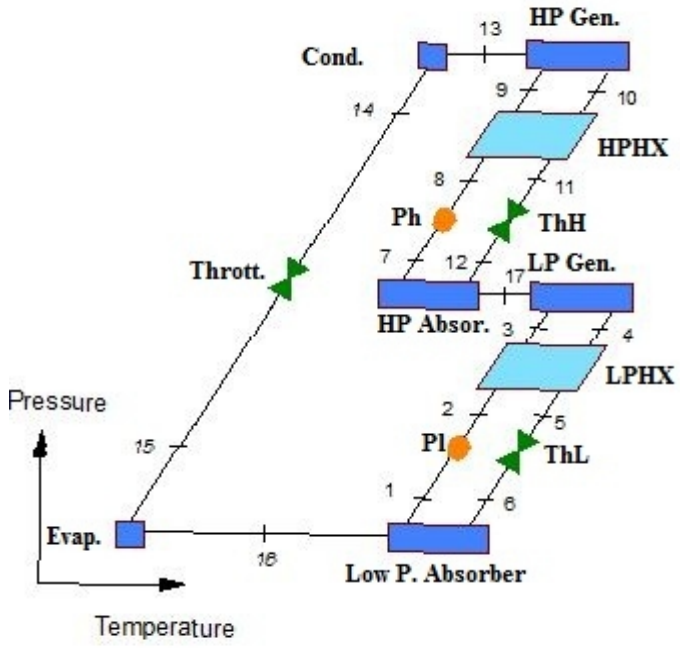

Figure 1 -Block diagram of Half Effect Vapour Absorption Refrigeration System

However, the absorbent that is the lithium bromide aqueous solution is circulated within two distinct stages i.e. the LP stage between the LP generator and the LP absorber, and the HP stage between the HP generator and the HP absorber. Compared to a single-stage vapour absorption refrigeration system, there are two additional components namely LP generator and HP absorber, in a half effect system. These are utilized to concentrate the lithium bromide aqueous solution in the LP stage cycle.

Table 1: p-t-x data for Half effect vapour absorption system

State point	P	T	X	Working fluid state
1.	PE	TAL	X_{Sl}	Equilibrium strong solution LP side
2.	PI	TAL	X_{Sl}	Strong solution
3.	PI	T3	X_{Sl}	Pre heated strong solution
4.	PI	TGL	X_{Wl}	Equilibrium weak solution LP side
5.	PI	T5	X_{Wl}	Sub cooled weak solution
6.	PE	T6	X_{Wl}	Sub cooled weak solution
7.	PI	TAH	X_{Sh}	Equilibrium strong solution HP side
8.	PC	TAH	X_{Sh}	Strong solution
9.	PC	T9	X_{Sh}	Pre heated strong solution
10.	PC	TGH	X_{Wh}	Equilibrium weak solution HP side
11.	PC	T11	X_{Wh}	Sub cooled weak solution
12.	PI	T12	X_{Wh}	Sub cooled weak solution
13.	PC	T13	0	Superheated refrigerant vapour
14.	PC	TC	0	Saturated refrigerant liquid
15.	PE	TE	0	Two phase refrigerant
16.	PE	TE	0	Saturated vapour refrigerant
17.	PI	T17	0	Superheated refrigerant vapour

2.1 Assumptions :

In direction to simulate these absorption refrigeration systems, several assumptions are made, comprehend the succeeding. [5]:

- The analysis of the system is prevailed under steady state conditions.
- The refrigerant (i.e., water) at the exit of the condenser is assumed to be the saturated liquid.
- The refrigerant (i.e., water) at the exit of the evaporator is assumed to be the saturated vapour.
- The Lithium bromide solution at the exit of the absorber is a strong solution and it is at the absorber temperature.
- The exit temperatures from the generator and the absorber from corresponding to equilibrium conditions of the separation and mixing particularly.
- The pressure losses in the pipelines and all the heat exchangers are assumed to be negligible.
- Heat exchange between the surroundings and the system, other than in that is prescribed by heat transfer at the absorber, generator, condenser, evaporator, do not appear.
- The reference state for the system is assumed water at an environment temperature To25°C and 1 atmospheric pressure (Po).
- The system exhibit chilled water.
- The half effect system rejects heat to cooling water at the absorber and the condenser.

2.2 Mass Conservation:

The mass conservation law applied for each component is written as:

$$\sum m_i = \sum m_e \qquad (1)$$

This law applied for each component of the cycle is written as:

$$.m_1 = m_2 = m_3 \qquad (2)$$

$$m_4 = m_5 = m_6 \qquad (3)$$

$$m_7 = m_8 = m_9 \qquad (4)$$

$$m_{10} = m_{11} = m_{12} \qquad (5)$$

$$m_{13} = m_{14} = m_{15} = m_{16} = m_{17} \qquad (6)$$

LP generator or LP absorber

$$. \quad m_3 = m_4 + m_{17} \qquad (7)$$

HP generator or HP absorber

$$. \quad m_9 = m_{10} + m_{13} \qquad (8)$$

2.3 Conservation of concentration:

The law justifying the concentration conservation for each component is written as:

$$\sum m_i X_i = \sum m_e X_e \qquad (9)$$

Where m is the mass flow rate in the system and X the is mass concentration of lithium bromide in the solution. The law is applied for each component of the cycle is written as:

LP generator or LP absorber

$$m_3 X_3 = m_4 X_4 \qquad (10)$$

HP generator or HP absorber

$$m_9 X_9 = m_{10} X_{10} \qquad (11)$$

$$X_1 = X_2 = X_3, \qquad (12)$$

$$X_4 = X_5 = X_6, \qquad (13)$$

$$X_7 = X_8 = X_9, \qquad (14)$$

$$X_{10} = X_{11} = X_{12}, \qquad (15)$$

$$X_{13} = X_{14} = X_{15} = X_{16} = X_{17} = 0. \qquad (16)$$

3. CALCULATION FOR THE HALF-EFFECT SYSTEM (HVARS):

The computer program is coded in Engineering Equation Solver (EES) for the thermodynamic analysis of HVARS.

In the analysis of this cycle the following assumption is considered

1. The pumping is isentropic
2. Across Solution expansion valve entropy change is neglected and temperature is also constant.

3.1 Input Parameters:

The following are the input parameters to half effect system:

Condenser Temperature TC = 38°C
Evaporator Temperature TE = 7°C
High Pressure side Generator Temperature Tgh = 80°C
Low Pressure side Generator Temperature Tgl = 80°C
High Pressure side Absorber Temperature Tah = 38°C
High Pressure side Absorber Temperature Tah = 38°C
Refrigeration Capacity Qe = 25 kW
Intermediate Pressure Pi = 4.953 kPa
Effectiveness of high pressure side solution heat exchanger EHXh = 0.7
Effectiveness of low pressure side solution heat exchanger EHXl = 0.7

4. CALCULATION OF FLAT PLATE COLLECTOR AREA:

The area of the flat collector is calculated on the basis of the requirement of heat in the two generators. The heat required in the two generators is calculated by the computer based EES program with input parameters given above.

4.1 Flat Plate Collector Specifications:

Dimensions = 2.005mm x 1.505m
Gross Area (A_F) = 3 m^2m
Efficiency (K) = 0.85
Cost = Rs. 6000
The Energy absorbed by the flat plate collector is given as [8] :

$$Q = K \times S \times A \quad (17)$$

Where,

K = efficiency of collector plate (K = 0.85)
S = average solar heat falling on earth's surface = 6 kwhr/ m2/day = 250 W/m2
A=Area of Flat Plate collector.

4.2 Calculation Of Area Of Flat Plate Collector For High Pressure Generator

Heat required in the high pressure generator of the system,
Qgh = 27.48 kW = 27480 W
Hence, the approx. area of the flat plate collector necessary for providing this much amount of energy is given by
= 27480 / (250 × K)= 27480 / (250 × 0.85)
= 129.32 m^2(i.e.,130 m^2)

Area of Flat Plate collector used in high pressure side (Ah) = 130 m^2

4.3 Calculation Of Area Of Flat Plate Collector For Low Pressure Generator :

Heat required in the low pressure generator of the system,
Qgl = 32.65 kW (i.e, 32650 W)

Hence, the approx. area of the flat plate collector necessary for providing this much amount of energy is given by
= 32650 / (250 × K)= 32650 / (250 × .85)
= 153.6 m^2(i.e.,154 m^2)

Area of Flat Plate collector used in high pressure side **(Al)= 154 m^2**

4.4 Total Area Of Flat Plate Collector (A) :

A = Ah + Al
A = 130 + 145
A = 284 m^2

4.5 Number Of Flat Plate Collectors Required :

Number of Flat Plate Collectors required in High Pressure Side (N1)
N1 = Ah/ A_F = 130/3 = 43.33
N1 = 44 Plates

Number of Flat Plate Collectors required in Low Pressure Side (N2)
N2 = Al/ A_F = 154/3 = 51.33
N2 = 52 Plates

5. RESULTS :

The variation of various parameter with respect to generator temperature (TG in °C) at different temperature of condenser (TC) is shown as :

5.1 COP:

The variation of COP with generator temperature is shown in Figure 2. The high values of COP are hold at high generator temperature and low condenser temperature. For a assumed condenser and evaporator temperature, there is a minimum temperature of generator, which address to the maximum COP. It should be noticed that the COP initially show the significant increase with an increase of generator temperature, and then the slope of the COP curves gets almost flat. In other words, increasing the generator temperature higher than a fixed value does not contribute to much improvement for the COP.

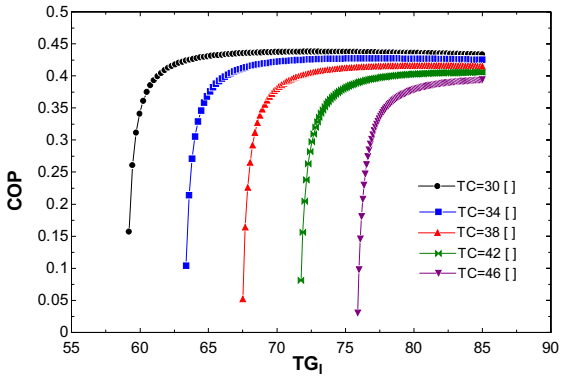

Figure 2 -Coefficient of performance (COP) versus generator temperature (TG in °C) and condenser temperature (TC) at (TE = 7°C)

5.2 Area of flat plate collector on High Pressure side (Ah) :

The variation of Area of flat plate collector on high pressure side is shown in Figure 3. As the generator temperature increases the Ahincreases linearly. When the condenser temperature is increased the value of Ah also increases. In the present study, where the evaporator temperature is maintained fixed at 7°C and condenser temperature is 38°C, generators temperature is 80°C the value of Ah is 130 m^2.

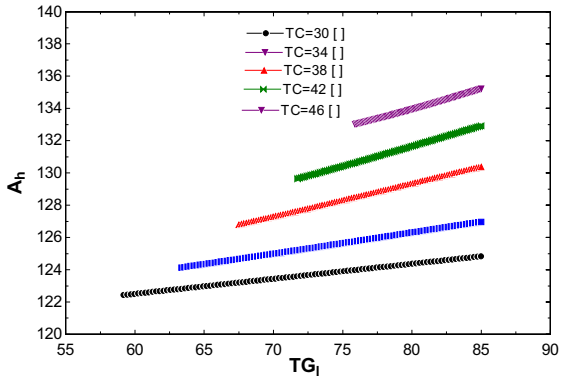

Figure 3 Area of flat plate collector on High Pressure side (Ah in m^2) versus generator temperature (TG in °C) and condenser temperature (TC) at (TE = 7°C)

5.3 Area of flat plate collector on Low Pressure side (Al) :

The variation of Area of flat plate collector on low pressure side is shown in Figure 4. The Al of the absorption cooling system drops keenly to a minimum value with an increase in temperature of generator and then further it approximately remains constant. In the present study, where the evaporator temperature is maintained fixed at 7°C and condenser temperature is 38°C, generators temperature is 80°C the value of Al is 154 m^2.

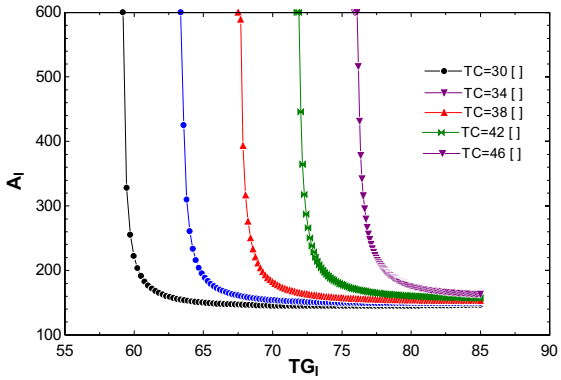

Figure 4 Area of flat plate collector on Low Pressure side (Al in m^2) versus generator temperature (TG in °C) and condenser temperature (TC) at (TE = 7°C)

5.4 Total Area of flat plate collector (A) :

The variation of Total Area of flat plate collector is shown in Figure 5. The A of the absorption cooling system drops keenly to a minimum value with an increase in temperature of generator and then further it approximately remains constant. In the present study, where the evaporator temperature is maintained fixed at 7°C and condenser temperature is 38°C, generators temperature is 80°C the value of A is 284 m^2.

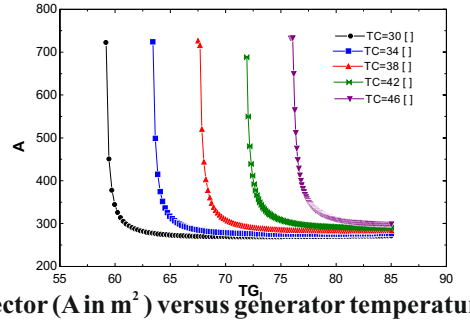

Figure 5 Total Area of flat plate collector (A in m^2) versus generator temperature (TG in °C) and condenser temperature (TC) at (TE = 7°C)

6. CONCLUSIONS:

The main results obtained are concluded below:

- Higher temperature of evaporator and generator, results in higher COP of the system due to the fact that as generator temperature increases, the heat transfer to the solution available in the generator increases, which results in the increase of mass flow rate and so does the COP.

- For the given temperature of condenser there is an optimum temperature of generator for which the total area flat plate collector is minimum. This optimum generator temperature comes out to be 80°C. This generator temperature gives the maximum COP.

- There exists a specific generator temperature below which a half effect system ceases to work. In the present work, this value is found to be 67.51°C, corresponding to an intermediate pressure of 4.953 kPa (for TC = Tal =Tah = 38°C, TE = 7°C and Tgh = Tgl = 80°C).

- For these values the Area of flat plate collector on High Pressure side (Ah) is 130 m2.Area of flat plate collector on Low Pressure side (Al) is 154 m2. Total Area of flat plate collector (A) is 284 m2.

REFERENCES :

[1] Abdulateef, J.M., 2008, Review on solar-driven ejector refrigeration technologies. Renew Sustain Energy Rev.

[2] Rabah GOMRI , (2010). Solar Energy to Drive Half-Effect Absorption Cooling System, Int. J. of Thermal & Environmental Engineering, Volume 1, No. 1 , 1-8.

[3] Jhalak Raj Adhikari, BivekBaral, Ram Lama, Badri Aryal, and Roshan Khadka , 2012, Design and analysis of solar absorption air cooling system for an office building Design and analysis of solar absorption air cooling system for an office building, Rentech Symposium Compendium, Volume 2, December.

[4] Akhilesh Arora, Manoj Dixit, and S. C. Kaushik, 2016, Computation Of Optimum Parameters Of A Half Effect Water-Lithium Bromide Vapour Absorption Refrigeration System, Journal of Thermal Engineering, Vol. 2, No. 2, pp. 683-692, April.

[5] Saeed. Sedigh , Hamid. Saffari, 2011, Thermodynamic Analysis Of Single Effect And Half Effect Absorption Refrigeration Systems, International Journal of Energy & Technology Vol. 3 pg 1-9.

[6] Absorption Chillers and Heat Pumps, Second Edition, By Keith E. Herold, Reinhard Radermacher, Sanford A. Klein, 1994.

[7] Jianzhao Wang, Danxing Zheng ,2009, Performance of one and a half-effect absorption cooling cycle of H2O/LiBr system, Energy Conversion and Management Vol. 50, pg 3087–3095.

[8] V.K.Bajpai, 2012, Design of Solar Powered Vapour Absorption System Proceedings of the World Congress on Engineering 2012 Vol IIIWCE 2012, July 4 – 6, London, U.K.

[9] Refrigeration And Air Conditioning, Third Edition, published by Tata McGraw-Hill Education private Limited, 2012 By C.P. Arora.

[10] Z.F. Li, K. Sumathy, 2000, Technology development in the solarabsorption air-conditioning systems, Renewable and Sustainable Energy Reviews, Vol. 4 pg 267±293.

[11] V Mittal, K S Kasana and N S Thakur, 2006, Modelling and simulation of a solar absorption coolingsystem for India, Journal of Energy in Southern Africa Vol 17 No 3 August.

[12] K. Sumathy , Z. C. Huang And Z. F. Li , 2002, Solar Absorption Cooling With Low Grade Heat Source —A Strategy Of Development In South China, Solar Energy Vol. 72, No. 2, pp. 155–165.

Numerical Analysis Of Forced Convection In A Lid Driven Cavity With Different Heat Source Locations Along The Bottom Wall

Divyaj Shah[1] ‡, Ketaki Godbole[2], C. M. Sewatkar[3]

1 Mechanical Department, College of Engineering, Pune, 232/3 Armamnet Estate, Necklace area, Pashan, Pune -411021, divyajshah28@gmail.com

2Mechanical Department, College of Engineering, Pune, 79, Saikripa society, Dhankawadi, Pune -411043, ktkgodbole.kg@gmail.com

3Mechanical Department, College Engineering, Pune, cms.mech@coep.ac.in

‡ Divyaj Shah; Tel: +91 99753 12842

ABSTRACT

The lid driven cavity problem is a standard tool for investigations of heat and fluid flow problems. Many researchers have studied the effects on heat transfer in a shear driven cavity with mixed convection. In the present work an in-house code is developed to carry out the simulations for a lid driven cavity which is under forced heat convection. The bottom wall is heated with various positions of heat location such as extreme left, left middle, middle, right middle and extreme right. Remaining part of the bottom wall and all other walls are thermally insulated. The vertical walls and the bottom wall have a no slip boundary condition. The top boundary is moving at a constant velocity. A Finite Volume semi explicit method is employed to study the effects of Prandtl number (Pr 0.71, 9.47 and 56) and Reynolds number $10 \leq Re \leq 400$. It is observed that an increase in Prandtl number greatly affects the heat transfer by decreasing the boundary layer thickness and thus increasing the temperature gradient. An increase in Reynolds number changes the flow field by creating a secondary vortex in the bottom rightcorner of the cavity. By moving the heat source from left to right the effect of temperature on the flow is studied and it is observed that a single isothermal cell is formed near the right wall and as the heat source is moved towards the right, the flow field influences the formation of the isothermal cell.

Keywords - Finite volume method, semi explicit method, Lid driven cavity, forced convection

1. NOMENCLATURE

A	Surface area (m^2)
K	Thermal Conductivity (W/mK)
L	Cavity side length
Pr	Prandtl number
Re	Reynolds number
T	Temperature (K)
U, V	Dimensionless velocities in x and y direction
Q	Heat flux (W/m^2)
x, y	Cartesian coordinates (m)
X, Y	Dimensionless Cartesian coordinates

GREEK SYMBOLS

Δ	Step size
Θ	Dimension less temperature
v	Kinematic viscosity (m^2/s)

2. INTRODUCTION

Lid-driven cavity flow of Newtonian fluids is one of the most well-known problems in the Computational Fluid Dynamics.

Many applications involving heat transfer have been studied with the help of the lid driven cavity flow problem. This finds its use in the applications such as geothermal systems, lubrication technologies, turbine nozzles, chemical processes, solar energy system, nuclear reactors [1-4]. Mixed convection heat transfer in a cavity with thermal sources were studied in a series of papers by Papanicolaou and Jaluria [5]. These papers aimed at analyzing effect of Richardson and Reynolds number in the range 0-10 and 50-2000 respectively. It was observed that the average Nusselt number increases with an increase in Richardson number at fixed Reynolds number. Hsu and Wang [6] carried out a numerical study on mixed convection in a cavity with discrete heat sources placed along the bottom wall. It was observed that highest temperature gradients were located near the heat sources. An increase in Reynolds number at fixed Richardson number showed an increase in heat transfer rate. Przemyslaw and Piotr [7] observed that Prandtl number does not have an impact on flow field patterns but strongly influences temperature field and heat transfer.

Previous researchers have focused at the solution of this problem with uniform heat flux throughout the bottom wall. The present study focuses on the solution of forced convection with heat flux at different sections along the bottom wall.

3. THE PROBLEM DESCRIPTION

Figure 1 shows the computational domain for two-dimensional flow in a lid driven cavity with forced convection heat transfer. Fluid is treated as Newtonian and incompressible. The radiation heat transfer effects are neglected.

The transient governing equations for the fluid flow and heat transfer are the continuity, momentum and energy equation. These equations in the non-dimensional form are presented below.

$$\frac{\partial U}{\partial X}+\frac{\partial V}{\partial Y}=0$$

$$\frac{\partial U}{\partial \tau}+U*\frac{\partial U}{\partial X}+V*\frac{\partial U}{\partial Y}=-\frac{\partial P}{\partial X}+\frac{1}{Re}*\left(\frac{\partial^2 U}{\partial X^2}+\frac{\partial^2 U}{\partial Y^2}\right)$$

$$\frac{\partial V}{\partial \tau}+U*\frac{\partial V}{\partial X}+V*\frac{\partial V}{\partial Y}=-\frac{\partial P}{\partial Y}+\frac{1}{Re}*\left(\frac{\partial^2 V}{\partial X^2}+\frac{\partial^2 V}{\partial Y^2}\right)$$

$$\frac{\partial \theta}{\partial \tau}+U*\frac{\partial \theta}{\partial X}+V*\frac{\partial \theta}{\partial Y}=\frac{1}{(RePr)}*\left(\frac{\partial^2 \theta}{\partial X^2}+\frac{\partial^2 \theta}{\partial Y^2}\right)$$

Where U and V are the dimension less velocities in the X and Y directions respectively. P is the dimension less pressure and θ is the dimension less temperature. The non-dimensional variables and non-dimensional parameters are as described below:

$$X = \frac{x}{L} \quad Y = \frac{y}{L}, U = \frac{u}{U_t}, V = \frac{v}{U_t}, P = \frac{p}{\rho * U_t^2}$$

$$\theta = \frac{T - T_c}{T_h - T_c}$$

$$Re = U_t * \frac{L}{\vartheta} \quad \Pr = \frac{\vartheta}{\alpha}$$

Where L is the characteristic length and U_t is the characteristic velocity. The thermo-physical properties in the above equation are kinematic viscosity (ϑ) and thermal diffusivity (α)

These equations are solved using the boundary conditions such that the top lid moves with a constant velocity U from left to right and is thermally insulated. The other walls are assigned no slip boundary conditions and are thermally insulted as well. The fluid is constantly heated through bottom wall which is divided into 5 sections such as Extreme Left (EL), Left Middle (LM), Middle (M), Right Middle (RM) and Extreme Right (ER) with heat flux (Q) acting through one section each time in different cases. The remaining part of the wall is insulated.

The simulations are carried out for Pr = 0.71, 9.54, 56 and Re = 10, 100, 400. The Pr values considered correspond to air, water and industrial aniline.

Top wall:

$$Y = 1, 0 < X < 1, U = 1, V = 0, \frac{\partial T}{\partial Y} = 0$$

Bottom wall:

$$Y = 0, 0 < X < 1, U = 0, V = 0$$

$\frac{\partial T}{\partial Y} = \frac{Q}{K}$ (For the part with heat flux)

$\frac{\partial T}{\partial Y} = 0$ (Otherwise)

Right wall:

$$X = 1, 0 < Y < 1, U = 0, V = 0, \frac{\partial T}{\partial X} = 0$$

Left wall:

$$X = 0, 0 < Y < 1, U = 0, V = 0, \frac{\partial T}{\partial X} = 0$$

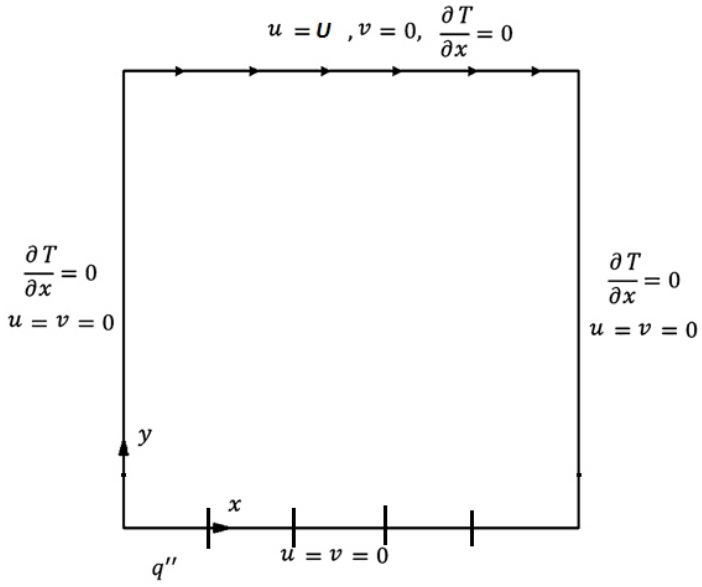

4. NUMERICAL DETAILS

The set of governing equations were discretized and solved by a finite volume semi explicit method [8]. A MATLAB code is developed to solve the momentum and energy equations. The momentum equation is solved in a two-step process in which an internal pressure correction loop is implemented to satisfy the continuity equation. The converged values of pressure are further used to calculate the correction velocities. These velocities are then added to the predicted velocities which are run to a specific convergence criterion.

The gird size used for the simulation is 101 x 101. The corresponding time step is in the range of $0.001 < \Delta t > 0.004$ as satisfied by the Courant–Friedrichs–Lewy (CFL) criterion. The convected variable at the center of each control volume face is calculated by using QUICK (Quadratic Upwind Interpolation for convective kinematics) scheme.

The code is validated against the results reported by Przemysław Błasiak1 and Piotr Kolasin´ski1 [7]. The case considered was a uniformly heated bottom wall with the upper lid moving. Excellent agreement is noticed and the comparison of plots for streamlines and isotherms showed one to one correspondence. The results for Re = 100 and Pr = 0.71 are shown in Figure 2.

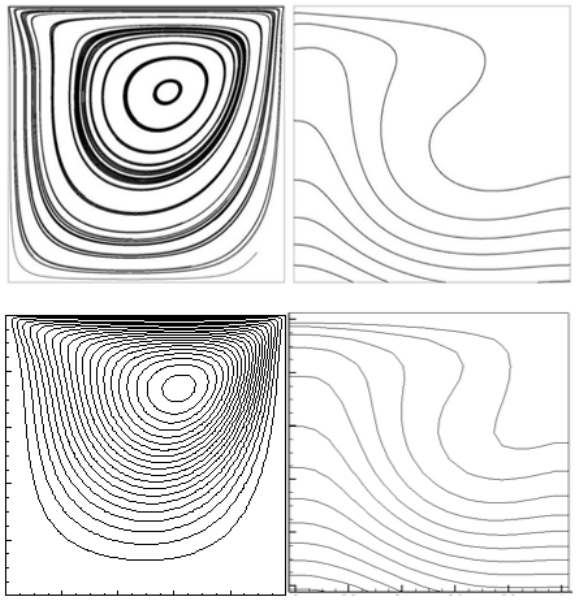

Figure 2: Comparison of results for Re = 100 and Pr = 0.71

5. RESULTS AND DISCUSSION

In the present study, streamlines and isotherms are presented to understand the effect of Reynolds and Prandtl numbers on fluid flow and hear transfer for each of the five sections of the bottom wall.

5.1 Effect of fixed Prandtl Number

The results for fixed Prandtl number (Pr=9.47) and $10 \leq Re \leq 400$ for the heat source acting through EL are shown in Figures 3 & 4. It is observed that an increase in Reynolds number affects the flow field such that the primary vortex is observed to move towards the right with an increase in Reynolds number. The nature of streamlines and isotherms is different at low Reynolds number. However, the contours show similar patterns at higher values of Reynolds number as shown in Figure 4.

5.2 Effect of fixed Reynolds Number

The streamlines and isotherms for Re=100 and $0.71 \leq Pr \leq 56$ are shown in Figures 5 and 6 for the heat flux acting through EL. The streamlines are observed to follow the same pattern for different values of Prandtl number as seen in Figure 5. The isotherms, on the other hand are observed to be influenced by the change in Prandtl number. It is thus clear that Prandtl number does not affect the flow field much but affects the heat transfer. For Prandtl number 0.71, the temperature contours occupy the domain of the grid space evenly but this occupied space reduces as the Prandtl number increases. With an increase in Prandtl number, the thickness of the boundary layer is observed to decrease. Consequently, the temperature gradient near the boundary increases with a decrease in thermal boundary layer.

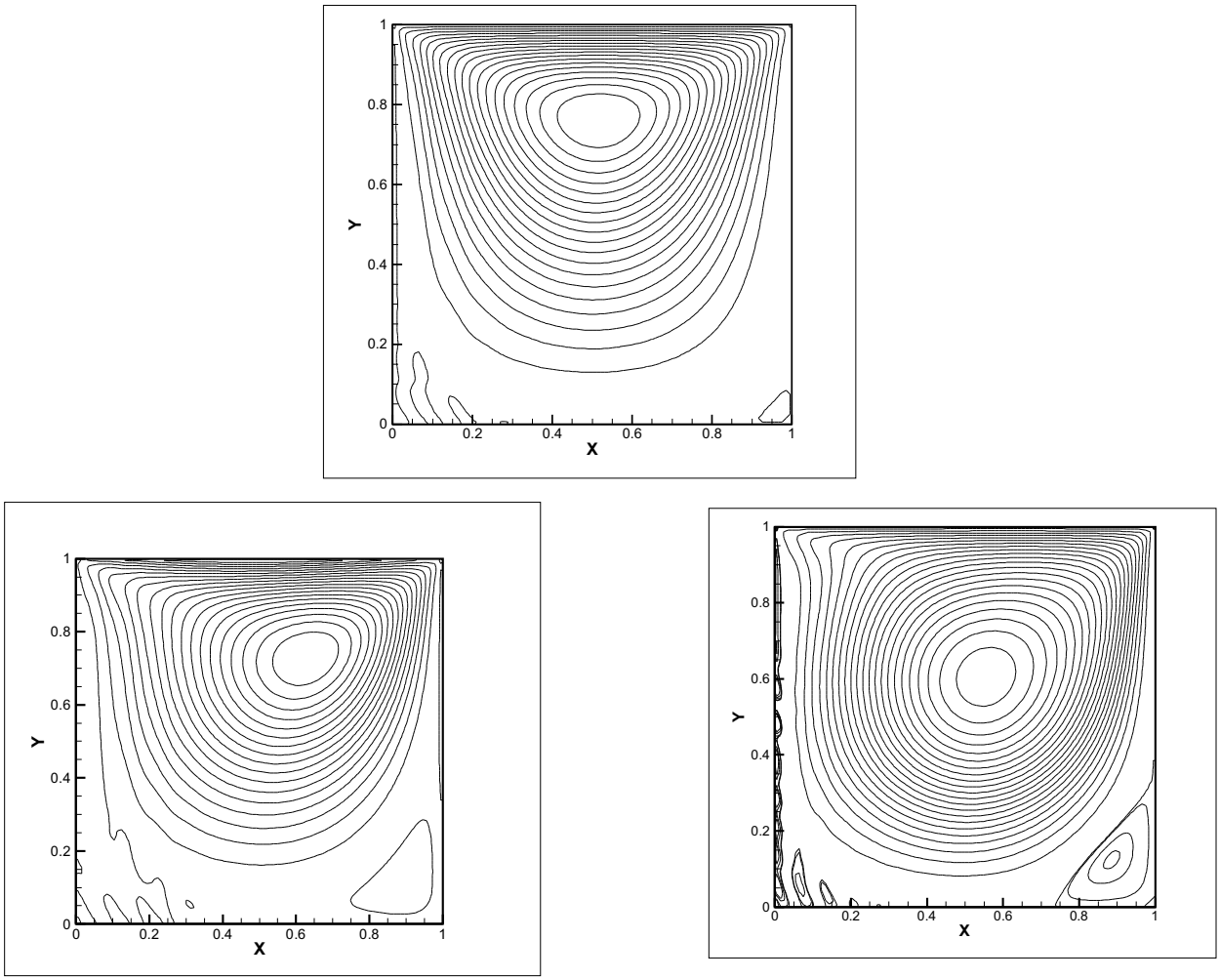

Figure 3: Comparison of streamlines for Reynolds number 10, 100 and 400 and Prandtl number 9.47

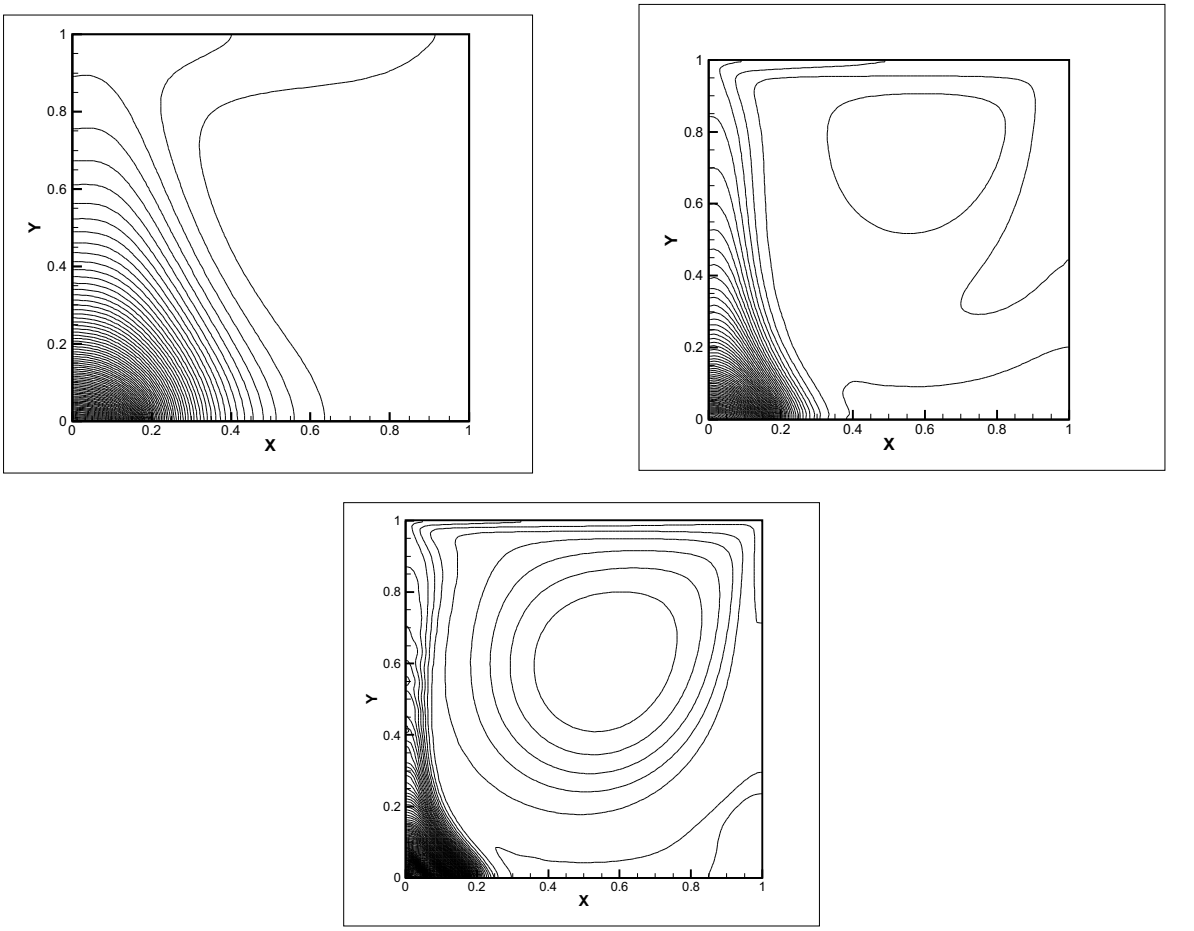

Figure 4: Comparison of Isotherms for Reynolds number 10, 100 and 400 and Prandtl number 9.47

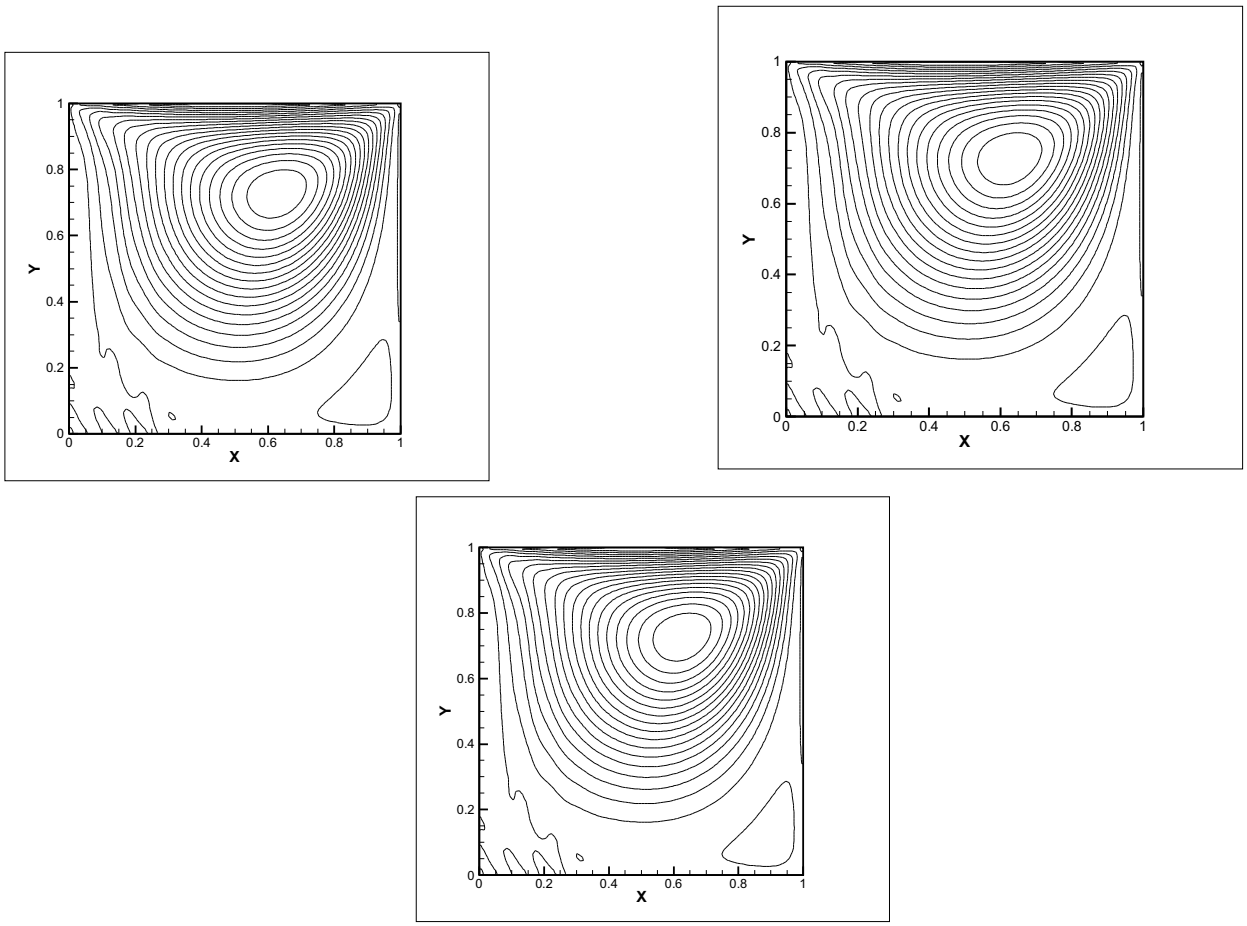

Figure 5: Comparison of streamlines for Prandtl number 0.71, 9.47 and 56 and Reynolds number 100

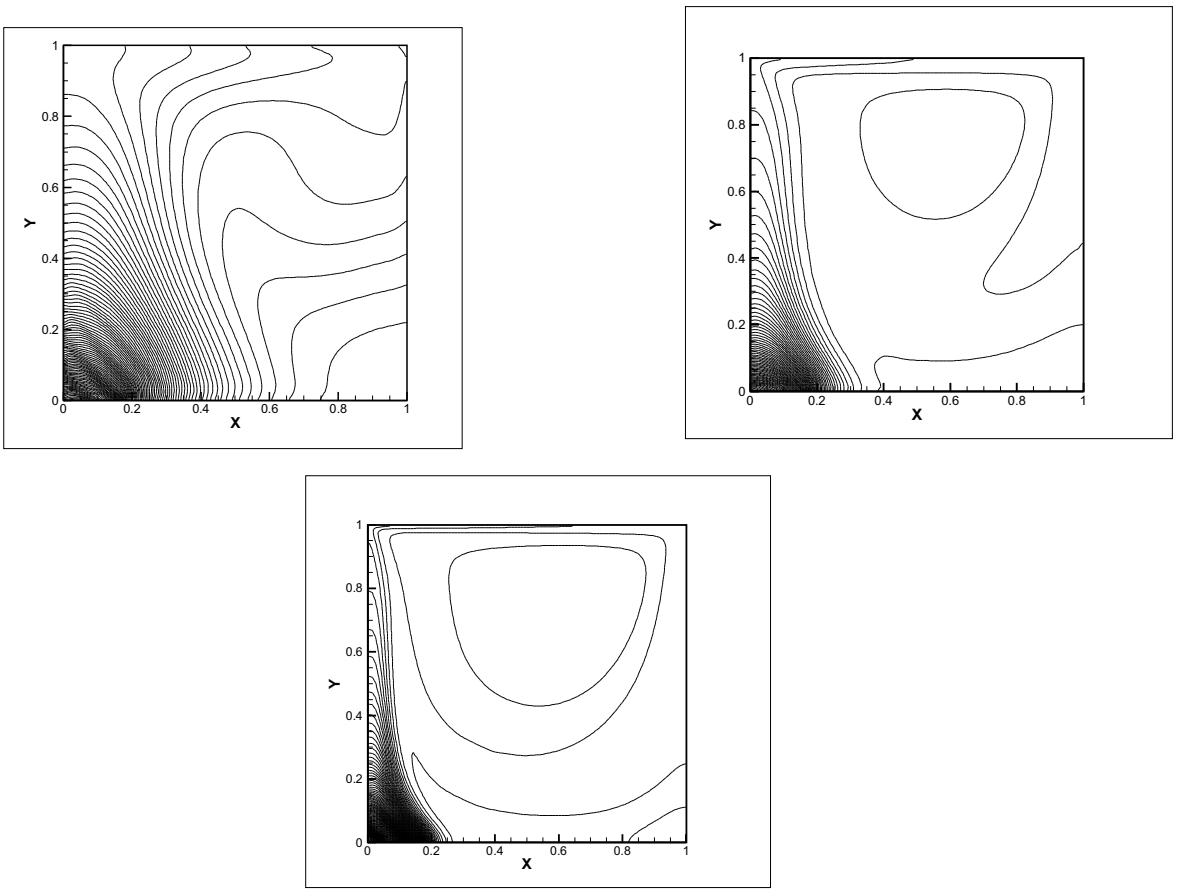

Figure 6: Comparison of isotherms for Prandtl number 0.71, 9.47 and 56 and Reynolds number 100

5.3 Effect Of Change In Location Of Heat Source

The streamlines and isotherms are also studied for a fixed value of Reynolds and Prandtl number by varying the position of heat source along the bottom wall. From Figure 8 it is observed that the streamlines are independent of the application of the heat source for fixed Reynolds and Prandtl number in forced convection. Figure 7 shows the comparison for isotherms for the same case. When the heat source is placed at the left most section (EL), the fluid which flows in the clockwise direction experiences colder fluid first and then interacts with the hot fluid. As the heat source is moved towards the right side, the fluid flowing carries hot fluid to the left uniformly. A small isothermal cell is seen to be formed near the right wall when the heat source is moved towards the right. This formation is influenced by the flow field moving in the clockwise direction.

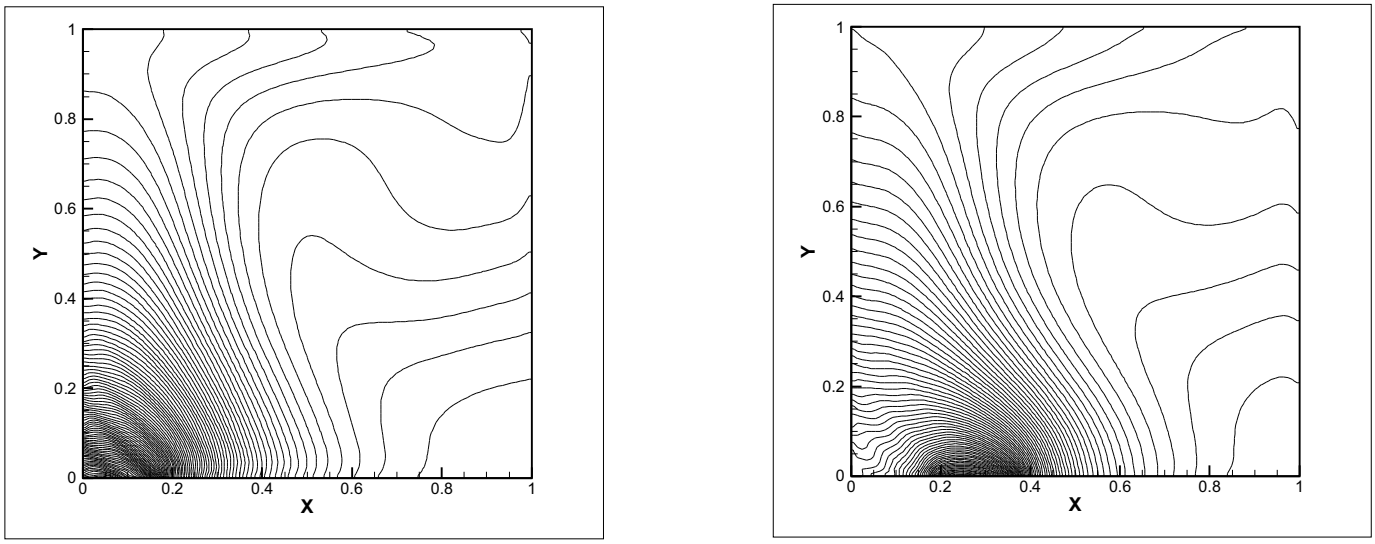

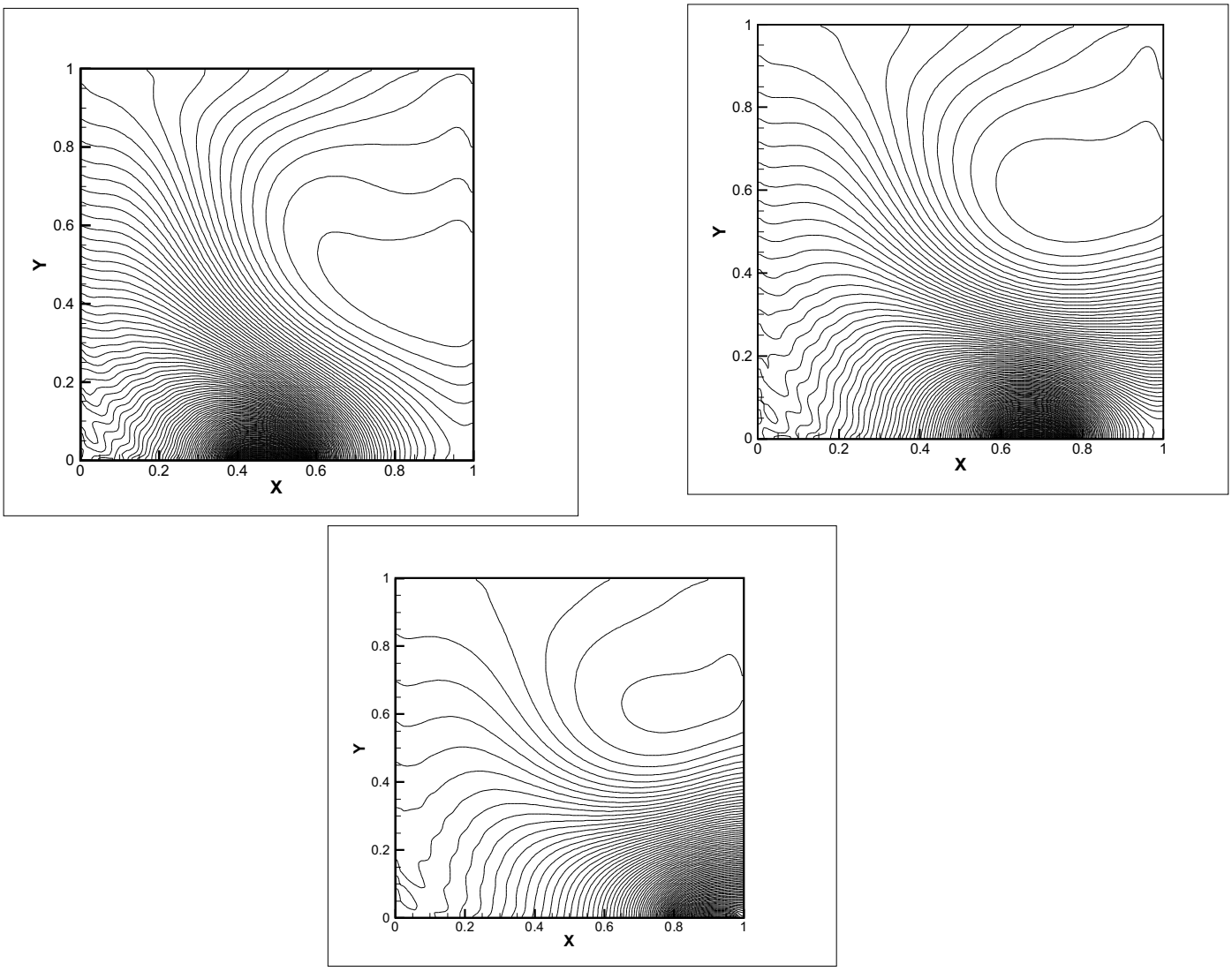

Figure 7: Comparison of isotherms for different locations of heat source for Re = 100 and Pr = 0.71

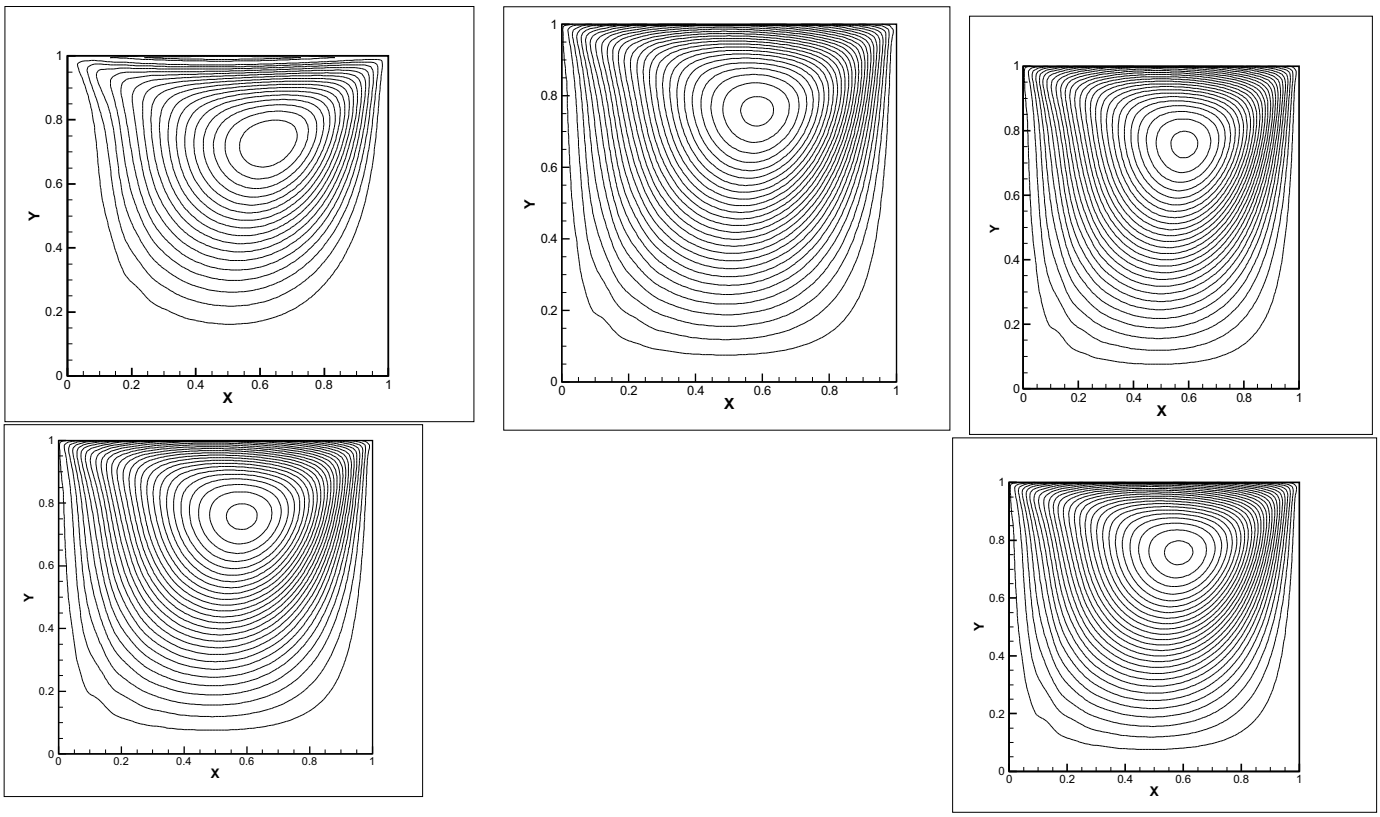

Figure 8: Comparison of streamlines for different locations of heat source with Re = 100 and Pr = 0.71

6. CONCLUSION:

The results for the numerical simulations are presented and studied for fluid flow and heat transfer in an insulated lid driven cavity with the heat source placed at different locations along the bottom wall. It is noticed that with an increase in Prandtl number the boundary layer thickness decreases and the temperature gradient increases at the boundaries. An increase in Reynold number causes the streamline patterns to change and move the primary vortex toward the right. A secondary vortex is seen to be formed at the right bottom corner with an increase in Reynolds number. Further, by moving heat source along the bottom wall, the streamlines show the similar pattern; however, single isothermal cell is seen to be formed near the right wall as the heat source is moved from left to right. As the heat source moves towards the right, the flow field influences the formation of the isothermal cell.

7. REFERENCES

1. *J.R. Koseff, A.K. Prasad, The lid-driven cavity flow: a synthesis of quantitative and qualitative observations, ASME J. Fluids Eng. 106 (1984) 390 - 398.*
2. *M. Morzinski, C.O. Popiel, Laminar heat transfer in a two-dimensional cavity covered by a moving wall Number, Heat Transfer 12 (1988) 265-273.*
3. *Shankar P, Despande DE (2000) Fluid mechanics in the driven cavity. Annu Rev Fluid Mech 32:93–136 4.*
4. *Bruneau CH, Saad M (2006) The 2d lid-driven cavity problem revisited. Comput Fluids 35:326–348*
5. *Papanicolaou E, Jaluria Y (1991) Mixed convection from an isolated heat source in a rectangular enclosure. Numer Heat Transf Part A 18:427–461*
6. *Hsu TH, Wang SG (2000) Mixed convection in a rectangular enclosure with discrete heat sources. Numer Heat Transf Part A 38:627–652*
7. *Przemysław Błasiak1 · Piotr Kolasin´ski1(2015) Modelling of the mixed convection in a lid-driven cavity with a constant heat flux boundary condition*
8. *Atul Sharma and V. Eswaran, A Finite Volume Method, Chapter12, pp. 445-482: Computational Fluid Flow and Heat Transfer, Edited by K. Muralidhar and T. Sundararajan, Narosa Publishing House, New Delhi, India and Alpha Science, UK, 2nd Revised Edition, 2003.*

Numerical Analysis of Wind Turbine Blade at Different Angle of Attack and Reynold Numbers Using Ansys

Mohammad Zunaid[1], Md. Gulam Mustafa[2‡], Nausad Ahmad Ansari[3]

[1]Department of Mechanical Engineer, Delhi Technological University, Bawana Road, Delhi-110042.

mzunaid3k@gmail.com, gm09mes31@gmail.com, naushad.nsr@gmail.com

[‡]Corresponding Author- Tel: +91-9312045421.

ABSTRACT

This paper work is on, how the lift force and drag force changes with different angles of attack and Reynold numbers for wind turbine blade. Analysis of wind turbine blade is done by using the NACA0012 air-foil profile . The Lift and Drag forces are computed at different angles of attack by varying from 5^0 to 75^0 for Reynold numbers ranging from 65,000 to 800,000 by ANSYS. The validations of the present work are done by comparing the results obtain from computation with the refined the mesh obtain by increasing the number of element. It is observed that results obtained by CFD analysis matches closely. Almost all CFD computation utilizes Navier–Stokes equations for its computation. From this CFD analysis, it is thus concluded that, with the increase of Reynold numbers, lift forces and drag forces increases. NACA0012 gives maximum lift and drag at larger Reynolds number.

Keywords- CFD; Air-foil; Drag Force; Lift Force; Angle of Attack; Reynold number

1. INTRODUCTION

Computational Fluid Dynamics has become an essential tool in almost every branch of fluid dynamics, is used in the development of aircraft, submarine, surface ship, and recently wind turbine. CFD utilises the numerical analysis and algorithm to solve and analyse the problem involving fluids, by computational methods, calculation is mainly to model the effect of liquid and gases with surfaces defined by boundary condition. The fundamental governing equations of CFD are the Navier-Stokes equations, which define the single phase fluid flow. In the early days two-dimensional methods were used to solve linear potential equations, like orthomorphic transformation of the flow over a cylinder to the flow about an air-foil. All CFD analysis is first started by defining the geometry of the product. However, for CFD the geometry, is the geometry where the fluid will flow [5], this means that it is important to define the boundaries for inlets, outlets, far-field conditions etc.

Lift Force, $L = \frac{1}{2} C_L \rho v^2 A$

Lift Coeffienct, $C_L = \frac{L}{1/2 \rho v^2 A}$

Drag Force, $D = \frac{1}{2} C_D \rho v^2 A$

Drag Coeffienct, $C_D = \frac{D}{\frac{1}{2} \rho v^2 A}$

Chris Kaminsky et al.[1]study is based on the VAWT with air-foil of NACA0012-34 aerofoil, with the help of Solid Work model, and imported in the STAR-CCM software for the CFD analysis. Two-dimensional air flow over the air-foil.2D and 3D simulations of thre air-foil is done using the different angle of attack ($0^0$to 15^0) and speed(15 to 30 mph). This study gave the stall angle is $8^0$for 2D and 3D gave no stall angle.

David Hartwanger et al. [2]research to develop a system, to assess multiple turbine installation using CFD analysis. They built NREL S809 air-foil wind turbine in two-dimensional and matched their results with 3D CFD

model. Created the cylindrical with geometry radius 2L and length 5L, for generation uses ANSYS, thus founded that with higher-resolution mesh generation; at high turbulence gavebetter result and it matches with experiment data of flow regime.

R S Amano et al. [3]research is based on the aerodynamic design of wind turbine rotor blade by CFD, and to optimize it.They uses Straight edge blade and Swept edge blade. In their work, they reasarch the way of increasing the efficiency of the blades at higher wind speeds, while maintaining the efficiency at the lower speeds of wind.Thus founded in their research that the swept edge geometry gave maximum efficiency at lowwind speed, and power is increased by 20% with the increase of wind speed by over 10 m/s.

Franck Bertagnolio et.al[4]explain the experimental and 2D CFD simulation result of NACA six digit wing section families, obtain the Ellipsys 2D provide better match result in both attache and stalled flow regime. The Ellipsys 2D CFD code uses Mentor shear stress transition turbulence model to predict turbulence effect in the laminar and turbulent regime.

S. Sarada et al.[5]worked on NACA 64618 air-foil, for the 2D and 3D CFD analysis, with the help of FLUENT code. The result of 2DCFD simulations shows that K-epsilon model do not provided satisfactory results in stalling regime and while the 3D CFD simulations shows satisfactory results in stalling regime.

Vance Dippold[6] has done series analyses to find performance of wall and different turbulence model, available in WIND CFD code. Thus concluded that turbulence models, i.e SST and K-e model work well with the neutral or favourable pressure gradient; however, in the SST model shows better result in the flow with adverse pressure gradient.

H.Gao et al. [7] have done analysis and CFD simulations to investigate unsteady 2D flow about the streamlined low speed GA(W)1 air-foil and corrugated dragonfly air-foil at Reynoldnumbers55000 to 68000.2D and 3D CFD simulations is done using unsteady Navier-Stokes solver. The work found that 2D and 3D simulation results is totally different at higher angles of attack and 3D CFD simulation results matches closely with the experimental data.

2. Geometry and Mesh Generation

In this CFD analysis, two-way velocity inlet method isused, in the C-type mesh. Figure 1 and Figure 2 shows the geometry of air-foil with the boundary condition. This mesh generation is done using ANSYS. Two mesh sizes having 100 and 40,000elements are used for analysis. Mesh having 100 elements defined as unrefined mesh and mesh size having 40,000 elements defined as refined mesh.

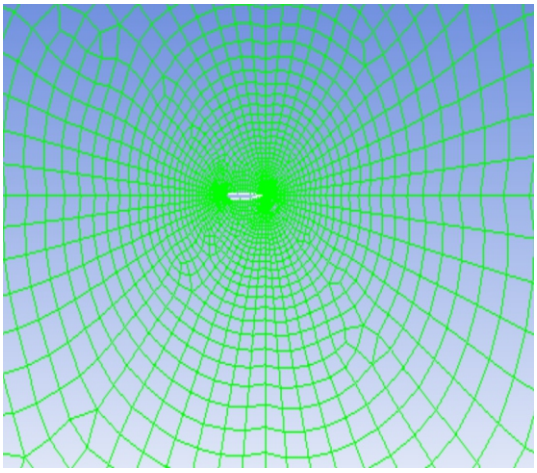

Figure 1. C- type Mesh

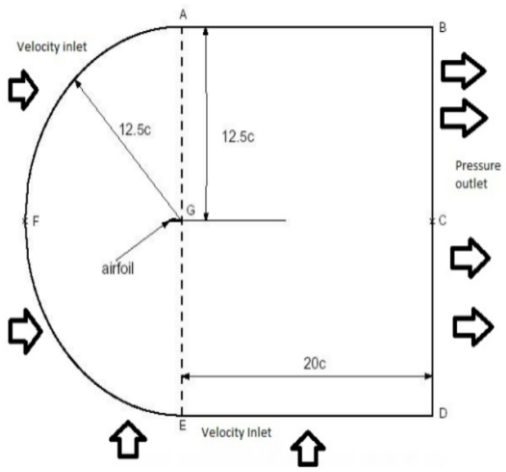

Figue 2. Geometry of Airfoil

3. Result and Discussion

Initially, CFD analysis is carried out for Reynolds number $6.5x10^4$, $1.5x10^5$, $5.0x10^5$ and $8.0x10^5$ and angle of attack of 5^0, 15^0, 25^0, 35^0,45^0, 55^0, 65^0,75^0.The results are shown in Figure 3-10 and Tables 1-4.

Table 1. CD and CL at various angle of attack at Re=65,000

Angle of attack	Unrefine C_D	Refine C_D	Unrefine C_L	Refine C_L
5	0.013	0.13	0.036	0.036
15	0.038	0.38	0.059	0.06
25	0.0615	0.087	0.0816	0.078
35	0.0831	0.15	0.101	0.118
45	0.102	0.124	0.117	0.12
55	0.118	0.122	0.129	0.13
65	0.13	0.15	0.14	0.15
75	0.43	0.168	0.17	0.142

Table 2. CD and CL at various angle of attack at Re=150,000

Angle of attack	Unrefine C_D	Refine C_D	Unrefine C_L	Refine C_L
5	0.043	0.05	0.036	0.036
15	0.038	0.038	0.059	0.044
25	0.615	0.082	0.081	0.078
35	0.0831	0.11	0.1	0.118
45	0.102	0.125	0.0816	0.09
55	0.18	0.126	0.059	0.56
65	0.1306	0.15	0.036	0.044
75	0.139	0.165	0.0116	0.02

Table 3. C_D and C_L at various angle of attack at Re=500,000

Angle of attack	Unrefine C_D	Refine C_D	Unrefine C_L	Refine C_L
5	0.038	0.05	0.0116	0.038
15	0.0615	0.037	0.0363	0.042
25	0.00831	0.084	0.0816	0.078
35	0.102	0.11	0.09	0.119
45	0.118	0.13	0.1	0.118
55	0.130	0.129	0.117	0.13
65	0.139	0.15	0.131	0.138
75	0.143	0.164	0.138	0.143

Table 4. C_D and C_L at various angle of attack at Re=800,000

Angle of attack	Unrefine C_D	Refine C_D	Unrefine C_L	Refine C_L
5	0.0134	0.052	0.143	0.15
15	0.038	0.038	0.138	0.147
25	0.06153	0.083	0.129	0.13
35	0.0831	0.11	0.117	0.118
45	0.1022	0.13	0.1	0.118
55	0.118	0.126	0.17	0.13
65	0.1306	0.148	0.129	0.138
75	0.139	0.141	0.138	142

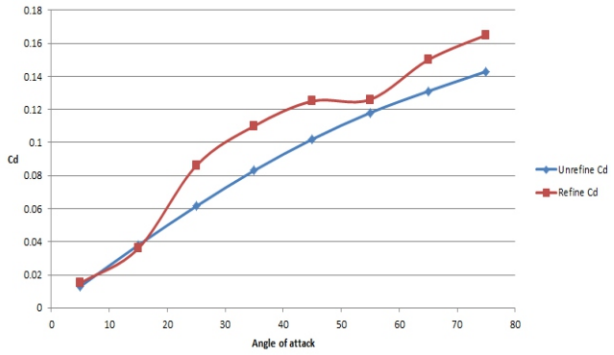

Figure 3. Graph of C_D vsAoA at Re=65,000

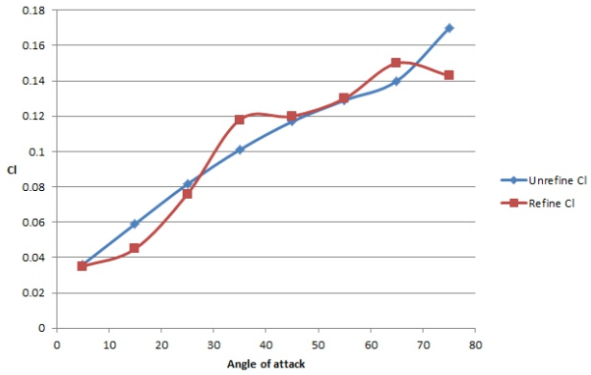

Figure 4.Graph of C_L vsAoA Re=65,000

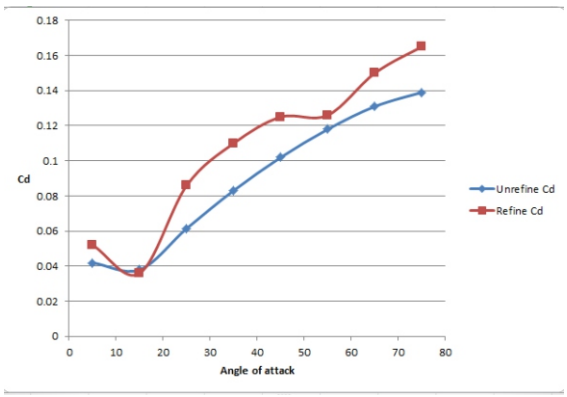

Figure 5. Graph of $C_D$vsAoA Re=150,000

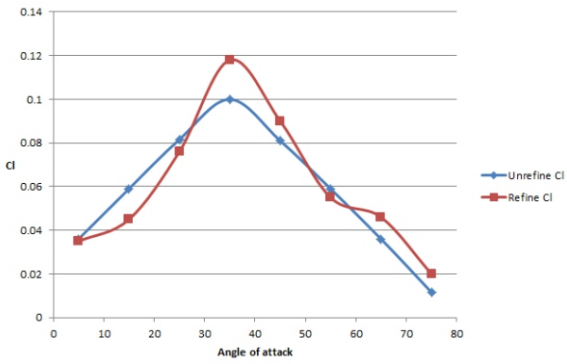

Figure 6. Graph of $C_L$vsAoA Re=150,000

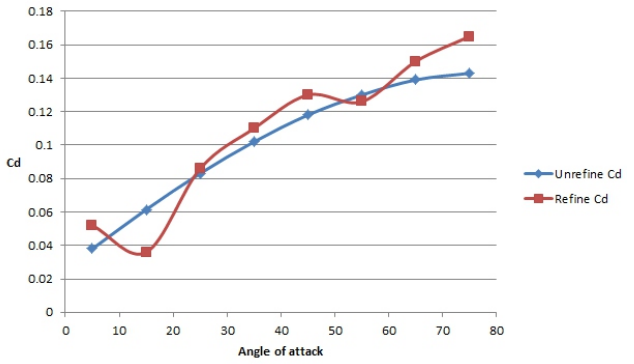

Figure 7. Graph of $C_D$vsAoA Re=500,000

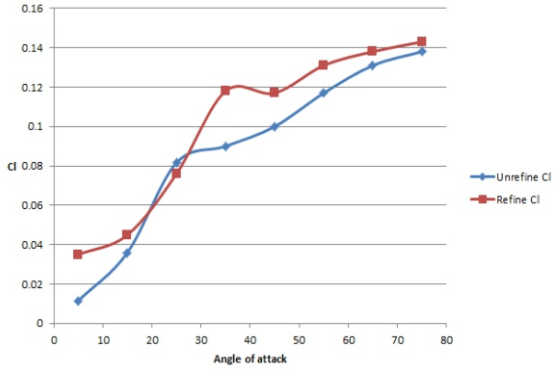

Figure 8.Graph of $C_L$vsAoA Re=500,000

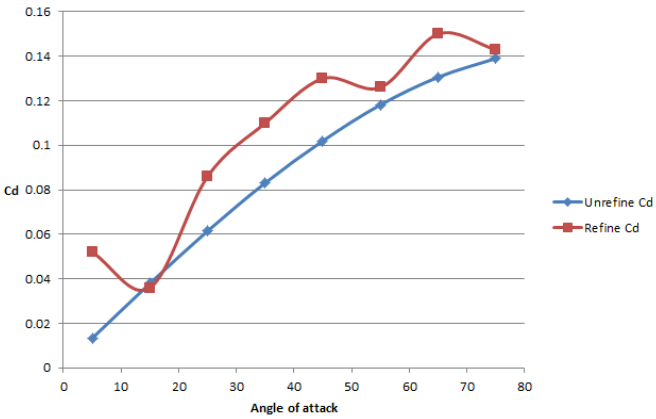

Figure 9. Graph of $C_D$vsAoA Re=800,000

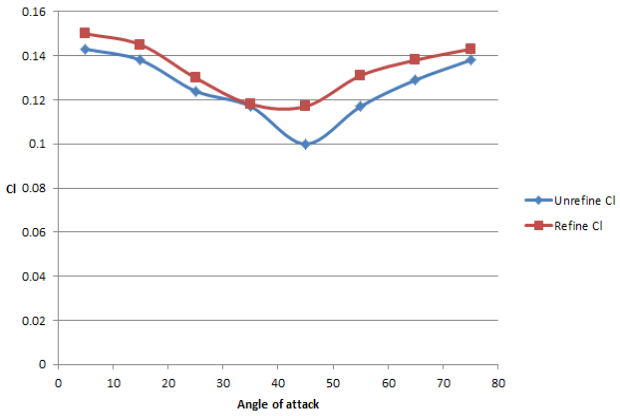

Figure 10. Graph of C_L VsAoA Re=800,000

From above graphs and tables we can conclude, that, for the lower angle of attack (5^0 to 25^0), results obtained in CFD simulation is distinct compared to experimental values. However, for angle of attack between (35^0 to 75^0) the value of C_L matches closely with refined mesh iteration. However, C_D values obtained by CFD simulation matches. The sudden decrease in C_L value occurs for Reynold Number=150,000.

4. Conclusion

- Validation of analysis is done by four Reynold number between 65,000 to 800,000 and eight different angles of attack between 5^0 to 75^0. It has been observed that, close matching in C_L and C_D values are obtained by CFD analysis in comparison to experimental values.

- It is found during the analysis,that C_L shows some deviation from experimental data at lower values of angles of attack, however, for higher angle of attack it closely match with experimental results.
- In general, it can be concluded that with the increase inReynold numbers, lift forces and drag forces increases. CFD simulation shows, NACA0012 provides highest lift force and drag force at higher Reynolds numbers.
- Thus, it can be concluded from the above simulation that in turbulent zone, efficiency of wind turbine is better than in laminar zone.

5. References

[1] Kaminsky, Chris, et al. "A CFD Study of Wind Turbine Aerodynamics."Conference, a CFD study of wind turbine aerodynamics, Ohio, USA. American Society for Engineering Education. 2012.

[2] Hartwanger, David, and Andrej Horvat. "3D modelling of a wind turbine using CFD." NAFEMS Conference, United Kingdom. 2008.

[3] Amano, R. S., and R. J. Malloy. "CFD analysis on aerodynamic design optimization of wind turbine rotor blades." World Academy of science, Engineering and technology 60 (2009): 71-75.
[4] Bertagnolio, F., Sørensen, N. N., Johansen, J., & Fuglsang, P. (2001). "Wind turbine airfoil catalogue". (Denmark.Forskningscenter Risoe. Risoe-R; No. 1280(EN)).
[5] Sarada, S., M. Shivashankar, and G. Rudresh. "Numerical Simulation of Viscous, Incompressible Flow around NACA 64618 Subsonic Airfoil Using Computational Fluid Dynamics." Advances n Mechanical Engineering (2010): 256.
[6] Dippold III, Vance. "Investigation of wall function and turbulence model performance within the wind code." 43rd AIAA Aerospace Sciences Meeting and Exhibit-AIAA-2005-1002. 2005.
[7]Gao, Haiyang, Hui Hu, and Z. J. Wang. "Computational study of unsteady flows around dragonfly and smooth airfoils at low Reynolds numbers." 46th AIAA Aerospace Sciences Meeting and Exhibit. 2008.
[8]Rainbird, J. M., J. Peiró, and J. M. R. Graham. "Blockage-tolerant wind tunnel measurements for a NACA 0012 at high angles of attack." Journal of Wind Engineering and Industrial Aerodynamics 145 (2015): 209-218.
[9]Ferrer, E., and X. Munduate. "Wind turbine blade tip comparison using CFD."Journal of Physics: Conference Series. Vol. 75. No. 1. IOP Publishing, 2007.
[10]Menter, Florian R. "Two-equation eddy-viscosity turbulence models for engineering applications." AIAA journal 32.8 (1994): 1598-1605.
[11]Abbott, Ira Herbert, and Albert Edward Von Doenhoff. Theory of wing sections, including a summary of airfoil data. Courier Corporation, 1959.

Triacylglyceride's Transesterification For Biodiesel: A Review

Amrik Singh[1‡], Amit Pal[1], Harwinder singh[1] and S.Maji[1],
[1]Department of Mechanical Engineering, Delhi Technological University, Delhi, India
[‡]Corresponding author: amriksingh200@gmail.com

ABSTRACT

Biodiesel can be produced from various oils or TAG's by transesterification in the presence of different catalyst. Biodiesel can be used either in pure form or blended form can be directly used in diesel engine without any modification or little modification. This review presents the transesterification of oil using different catalyst and their mechanism. Homogeneous and heterogeneous catalysts are discussed along with their advantages and disadvantages. This review also gives insight on the microwave heating of reactions and traditional method of heating of reactions. Apart from this use of enzyme based catalyst and current status is explained. Now a day's nano-size catalyst also gains much attention due to large surface contact area.

Keywords- Transesterification; Catalyst; Enzyme; Nanoparticle catalyst.

1. INTRODUCTION

There are many feedstock's from which biodiesel is obtained. This oil cannot be directly used to run engine due to high viscosity and low volatility which leads to injector coking and engine deposit [1,2]. However this problem is eliminated by transesterification of oil to alkyl ester [1, 3].

Transesterification is also called alcoholysis. Transesterification is reversible reaction in which triglycerides are converted to di-glycerides and to mono-glycerides which finally gives glycerol. Biodiesel floats at the top while glycerol sinks to the bottom which is separated easily [4]. In transesterification methanol and ethanol is mainly used as alcohol due to low cost. However octanol, propanol, butanol and tert butanol can also be used but their cost is higher as compared to methanol and ethanol [5,6,7,8]. If methanol is used in reaction then process is called methanolysis. General equation for transesterification is represented as in fig. 1 [9].

This reaction generally takes place in presence of catalyst which may be acidic or basic in nature as alcohol is scarcely soluble in oil, so catalyst increase the solubility, thus accelerates the reaction [4]. The transesterification process removes the glycerin, so viscosity decreases but heating value and cetane number does not change [10].

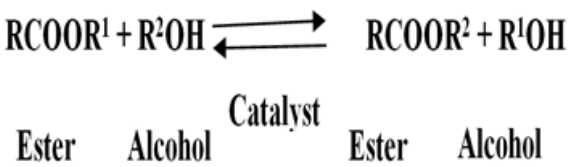

Figure 1: Transesterification Reaction

1.1. Kinetics of Transesterification Reaction

The oil from which biodiesel is produced is known as triglyceride (TAG). TAGs are formed by covalent bonding of carboxylic acid with alcohol. In this context, TAG is an ester formed by combining of three molecules of fatty acids covalently bonded with glycerol molecule [11]. Fatty acid has carboxylic group while glycerol has three hydroxyl group which while combining form ester or TAGs. Transesterificationis a chemical process in which

carboxylic acid ester is converted into different carboxylic acid esters.

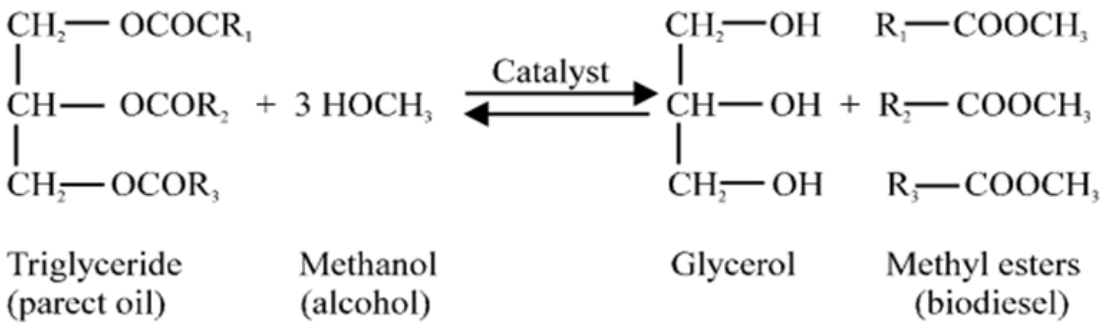

Figure2 Transesterification Reaction

2. Base-catalysed Transesterification

Base catalyst are mostly used for transesterification of vegetable oils [12,13,14,15,16]. When the tryglyceride contains free fatty acids or excess amount of water then acid catalyst are used to reduce the soap formation [13,16, 17]. Base catalyzed transesterification reaction is 4000 times faster then acid catalyzed reaction but it is used only if trygleceride contains less then 2% free fatty acids [18]. Sodium and potassium hydroxide are mostly used for industrial purpose.

2.1. Mechanism of Base Catalyzed Transesterification

The transesterification using base catalyst involves four step pre step or first step in which base reacts with alcohol and form protonated catalyst and an alkoxide. In the next step carbonyl group of oil is attacked by nucleophilic and forms intermediate [19, 20,12]. In third step alkyl ester and anion of diglyceride are formed. In fourth step the catalyst deprotonates, thus regenerating the base which again reacts with second molecule of alcohol and starts another cycle.

Base catalyst are mostly used because reaction takes place at low temperature and pressure that is 60°C and 20 psi and obtain high yield about 98%. However there are some shortcomings it requires high energy, to separate the catalyst from the media after transesterification pro-reaction treatment is required, difficult to recover glycerol after the reaction moreover it forms soap with free fatty acids.

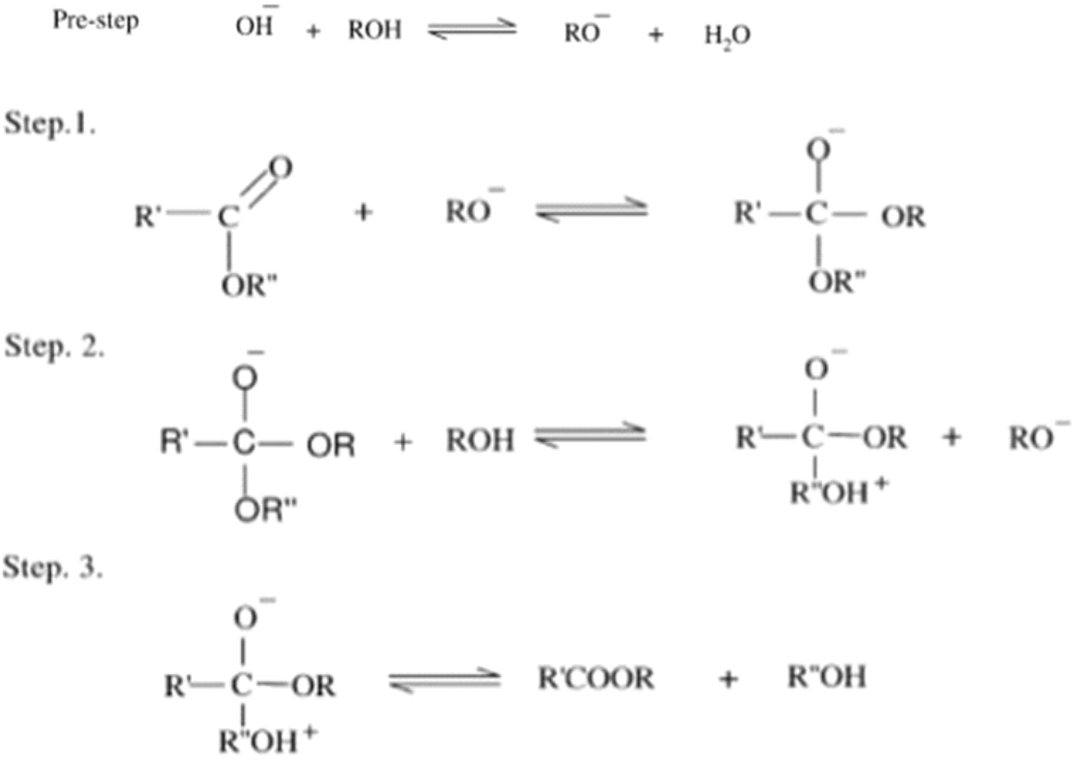

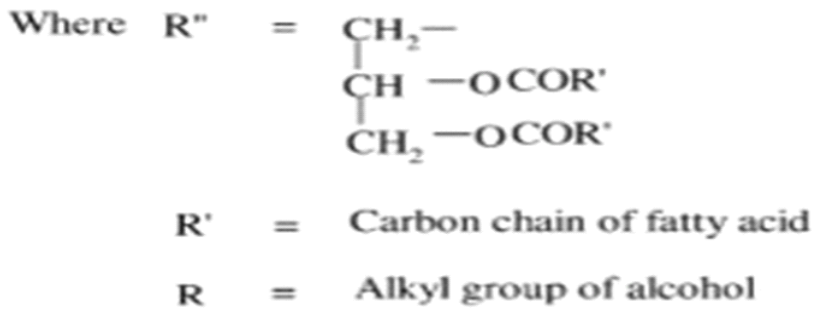

Figure 3 Mechanism for Base Catalyzed Transesterification Reaction

2.2. Factors Affecting Base Catalyzed Transesterification.

Effect of alcohol to oil molar ratio: the yield of methyl esters generally depends upon methanol to triglyceride molar ratio. Theoretically three moles of methanol are required per mole of oil for transesterification. A vegetable oil [21] studied the amount of alcohol required for transesterification of vegetable oil in terms of alcohol to oil molar ratio.

Shazia sultana [22] studied transesterification on five different molar ratios in the range 2:1 to 10:1 and obtained maximum yield 92% with 6:1 methanol to oil molar ratio.On further increase in methanol to oil molar ratio the ester yield decreases.

Encinar J.M et al [23] studied different ethanol to oil molar ratio between range 3:1 to 15:1 for the transesterification of cynarer oil and reported that reaction is incomplete when molar ratio is less than 6:1. The yield of ester increases as the molar ratio increased upto 12:1 and obtained optimum value at 9:1. However many authors reported that [24,25] with increase in methanol to oil molar ratio the yield decreases, for instance, Lu et al [24] worked on different molar ratio ranges from 1:1 to 1:10 and reported that the maximum yield is obtained at 1:1 and this may be due to inhibitory effect of alcohol on lipase activity.

Similarly Li et al [25] given same trend that with increase in molar ratio yield decreases, the achieved 95% yield in 12 hour at molar ratio 4:1.

2.3 Effect of Catalyst Concentration

Mostly alkaline, acid and enzyme catalyst are used. If the oil contains high free fatty acids and large quantity of water then acid catalyst is used for transesterification. Sultana Shazia [22] studied the effect of NaOH concentration between the range of 0.1-0.9 wt% and obtained that yield increases with increase in catalyst concentration from 0.1-0.5%. The yield decreases with further increase in NaOH concentration and reduced to 50% with 1.5% NaOH concentration. This is because with increase in the concentration of catalyst, soap formation will take place and reduce the yield with increase in viscosity. Ma F et al [27] studied the effect of NaOH and NaoME concentration and found that at 3% and 5% w/w of catalyst to beef tallow oil maximum yield is obtained.

3. Acid-Catalyzed Transesterification

The acid catalyzed transesterification does not gain much popularity because it is 4000 times slower than the alkali catalyzed reactions [18]. Its performance does not affected by the presence of free fatty acids and can catalyze simultaneously both esterification and trans-esterification. Acid catalyst can produce biodiesel from low cost feed stock having high free fatty acid FFA. The transesterification of triglyceride consist of three reversible reactions.

Acid catalyzed transesterification mechanism is shown in fig for monoglyceride. Carbonyl group protonation leads to carbocation which forms tetrahedral intermediate after the nucleophilic attack of alcohol. The glycerol

is separated and forms new ester. These reactions should be carried in the absence of water because carbocation reacts with water to form carboxylic acids.

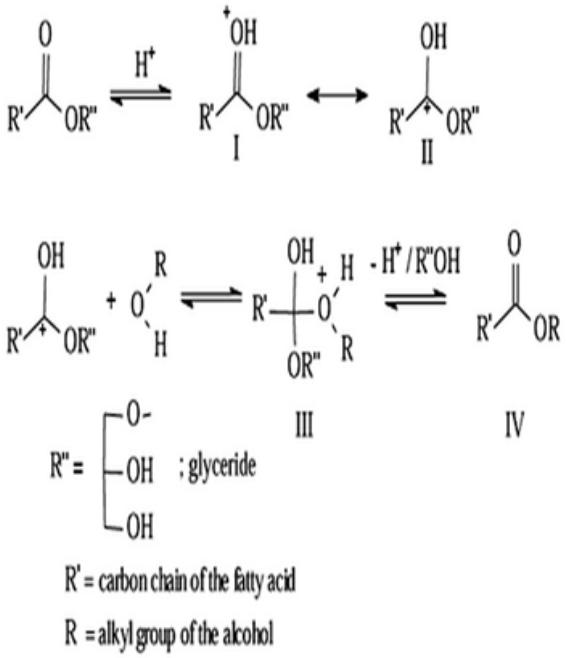

Figure 4. Mechanism of acid catalyzed reaction.

4. Catalyst for Transesterification Process

For transesterification following catalyst are investigated, heterogenous, enzymatic and homogenous or alkali catalyst like potassium and sodium hydroxide are mostly used in industrial transesterification because they promote reaction at low temperature also [28].

4.1. Homogenous Catalyst

Homogeneous catalysts are further divided as homogeneous acids and homogeneous base catalyst. Homogeneous base catalysts are commonly used for transesterification of triglyceride. Homogeneous base catalyst such as carbonates [29], alkaline metal hydroxide [30,31] and alkoxides [17, 32] are most commonly used [28] the alkoxide are more difficult to handle then hydroxide because alkoxide are hygroscopic in nature. Alkoxide does not form soap from triglyceride saponification due to the presence of hydroxide ion which act as an impurity in alkoxide [28]. While using alkaline catalyst the free fatty acid content should not increase 0.5% by wt. otherwise soap formation will takes place which hampers the production of biodiesel. Various authors reported that 90% yield is obtained by using potassium hydroxide and boiler ashes in the methanolysis and ethanolysis of coconut and palm oil [3323, 34, 35]. Ma et. al. [27] found that alkaline catalyst Naoh perform better than NaoMe. However to obtain higher yield the concentration of naome is slightly higher as compared to Naoh Ma et. al. [27]. Singh et al. [36] studied about alkaline catalyst (NaoH, KoH, KoMe and NaoMe) and found that better yield is obtained by potassium based catalyst as compared to sodium based catalyst. Where methoxide based catalyst produces higher yield compared to hydroxide based catalyst.

4.2. Homogeneous Acid Catalyst

For the transesterification of free fatty acid (FFAs) h**o**mogeneous acid catalyst are more effective as compared to base catalyst. Acid catlysed reactions proceed 4000 times slower than the base catalyzed reaction[15]. However acid catalyzed reactions have lower moisture sensitivity as well as non-appearance of soap formation. Acid catalysts are used where oil has higher FFAS [28]. If base catalyst are used it will form soap. Acid catalyzed reactions are two stage processes, in first stage esterification takes place in the presence of acid catalyst while in the second stage reaction takes place in the presence of base catalyst. The acid catalyst mostly used are, sulphonic

acid, organic sulfonic acid, hydrochloric acid, and phoshphoric acid. Freedman et al. [32] uses sulphuric acid as catalyst with alcohol oil ratio 30:1 and found that to obtain 90% yield reaction took 50h to complete at 65° C. Zullaikah et. al. [37] uses sulphuric acid as catalyst for the transesterification of rice bran oil between temperature range of 60-80°C.

4.3. Heterogeneous Catalyst

It is difficult to separate homogeneous catalyst from the reaction mixture so heterogeneous catalysts are developed. Heterogeneous catalyst. heterogeneous catalyst are advantageous because they does not form soap through saponification of triglyceride and eliminate corrosion problems and reaction requires high temperature and pressure. However there are some limitations like, they have poor performance compared to homogeneous catalyst, and due to less surface contact catalyst does not participate effectively in reaction so catalyst must be in porous state. The surface of heterogeneous catalyst must be hydrophobic in nature so that it adsorb triglyceride and to avoid adsorption of polar by products like water and glycerol on surface. Solid catalyst which are mostly used are, alkaline earth oxide, solid organic base, basic oxides supported, basic zeolite, insoluble metal salt and hydroxide, basic metal oxide, hydrotolerite and hetropolyacids [38].

4.3.1 Alkaline Earth Oxide

Ca and Mg are alkaline earth metals which are most widely used as heterogeneous base catalyst.Gryglewicz [31] found that alkali earth metal oxides sucessfuly catalyzed the transesterification reaction. Alkaline earth oxides are basic due to M^{2+} and O^{2-} ion pairs [39]. Various authors reported the use of Cao as catalyst for the transesterification of sunflower, and rapeseed oil with methanol [40, 41]. Moreover, strontium oxide, Cao, Mgo also investigated as catalyst for transesterification with high basicity [42, 43, 44].

Martyanov and Sayari [45] used calcium methoxide as catalyst for the transesterification of triglyceride and found that initially reaction is slower as compared to homogeneous sodium methoxide and magnesium methoxide, but at later stage the rate of reaction is higher than magnesium methoxide. Alkaline earth metal oxides assimilate with metal oxide and form composite oxide [46] which can be used as solid base catalyst for transesterification. Composite oxides are more stable and easy to separate from the reaction media.

4.3.2. Acid Zeolite

Zeolites are most widely used as solid acid catalyst for transesterification of oil and made hydrophobic by elimination of water of hydration. Shu et al, [47] uses La/Zeolite beta catalyst for the batch transesterification of soybean oil and found that La/Zeolite base catalyst have higher conversion rate than zeolite beta heterogeneous acid catalyst used in biodiesel production are mostly mesoporous [48, 49]. Subsume of microporous H-β-Zeolite with secondary mesoporosity create a heterogeneous solid catalyst which accelerates microalgae transesterification by reducing the diffusion barriers [50, 51] uses zeolite catalyst for the transesterification of waste cooking oil and found that yield is independent of porosity of zeolite and found that yield increases with increase in strength of the acid.

4.3.3. Hetropolyacids

Hetropolyacids attains much attention due to its superacidic nature (PK H^{+}> 12) and porous structure. They are highly soluble in polar media in their native form which make their contribution in reaction as homogeneous catalyst [52]. Chai et al, [53] uses heterogeneous catalyst ($CS_{2.5}$ $H_{0.5}PW_{12}O_{40}$) for transesterification of eruca sativa gars oil and obtained the same result as by using sodium hydroxide or sulphuric acid with one advantage of easy separation of catalyst from media and its reuse. Cao et al [54] use the hetroppolyacids ($H_{35}PW_{12}O_{40}$. $6H_2O$) catalyst for transesterification of waste cooking oil. In 10h 87% yield is obtained using hexhydrate catalyst. The

catalyst would be separated easily and was reused many times.

5. Microwave Irradiation Effect On Biodiesel Production

Traditionally organic reactions are heated by various equipments such as sand bath, heating jackets and oil baths. These techniques are not effective because they are slower and temperature gradient took place. But now a days microwave dielectric heating is preferred in microwave heating radiation passes the wall and only heat the solvent and reactants without heating the vessel [55].

Patil et. al., [56] used micro-algal oil to produce biodiesel by transesterification by heating with microwave radiation and observed that microwave irradiation effect the reaction in two way 1. reaction is boosted by thermal effect. 2. Vaporization of methanol due to strong microwave radiation. Ma et al, [57] observed that microwave heating reduce energy and reaction time due to volumetric heating.Ma et al, [57] produced biodiesel by transesterification of micro-algal oil in the presence of KOH by conventional heating and microwave heating method and find that with conventional heating system reaction completes in 210 minute while with microwave heating reaction completes in 5 min, obtained 96.54% conversion using KOH 1% wt, 1:8 oil to methanol at 65°C.

6. Nanoparticle Catalyst in Transesterification

For the conversion of triglyceride to methyl esters transesterification takes place in the presence of catalyst. Catalysts used are either base catalyst or acid catalyst. Base catalyzed reactions are much faster than that by acid catalyzed reaction. However basic catalyst have some drawbacks such as loss of catalyst, some catalyst remain in the biodiesel does not separated. To overcome this drawback heterogeneous catalyst are used but require long reaction time and large volume. Therefore, to improve the conversion of free fatty acid, lots of efforts are done to produce catalyst with high surface area. Highest methyl esters can be produced by catalyst with high surface area [58]. Many authors investigated that Nano sized catalyst have large contact area. For instance, Wang et. al., [59] produced biodiesel from waste cooking oil in the presence of nano-sized catalyst (Aluminum dode catungs to phosphate AIPW) and observed that ≈ 96% conversion was achieved at 55° C due to large surface area of nano paticle.

6.1. CaO/ MgO Catalyst

Calcium oxide is heterogeneous base catalyst mostly used for transesterification reaction. It has many advantages, such as easy availability, higher activity, reusability, low cost and mild reaction condition. Pretreatment temperature range between 700-1000 K is used to remove water and CO_2 which is adsorbed on the surface of CaO [60]. Most of the catalyst has adverse effect on yield of methyl ester in the presence of water. However CaO catalyst performs well in the presence of water, it forms methoxide ion in the presence of methanol which is highly active. Mechanism of transesterification with CaO as catalyst is given in fig [61].

As shown in equation 1, Ca^{2+} extracts OH^- and O_2^- extracts H^+ from water so they are easily extracted by reactants during chemical reaction. As shown in equation 2, methoxide anion and H_2O forms when OH^- extracts H^+ methanol. In equation 3 again O^{-2} extract H^+ and form surface methoxide anion. If water exceed by 2.8 wt% of oil it hydrolyze the methyl esters and forms fatty acid and methanol. Liu et. al., [61] obtained 95% yield at temperature 65° C by using CaO catalyst. Hsiao [75] used nano powder CaO as catalyst and obtained 96.6% yield at 1:6 oil to methanol ratio, reaction time 1 hour, 338 K temperature and 3 wt% catalyst.

Due to easy preparation and low cost researcher focus attention on MgO and CaO catalyst. Huaping [62] obtained 93% yield using CaO as catalyst. Di serio [63] achieved 92% yield by using MgO as catalyst. Dossin [64] use MgO as catalyst in batch work reactor and found that satisfactorily at ambient condition. Magnesium oxide is identified as good homogeneous catalyst for transesterification of ethyl acetate with methanol [64].

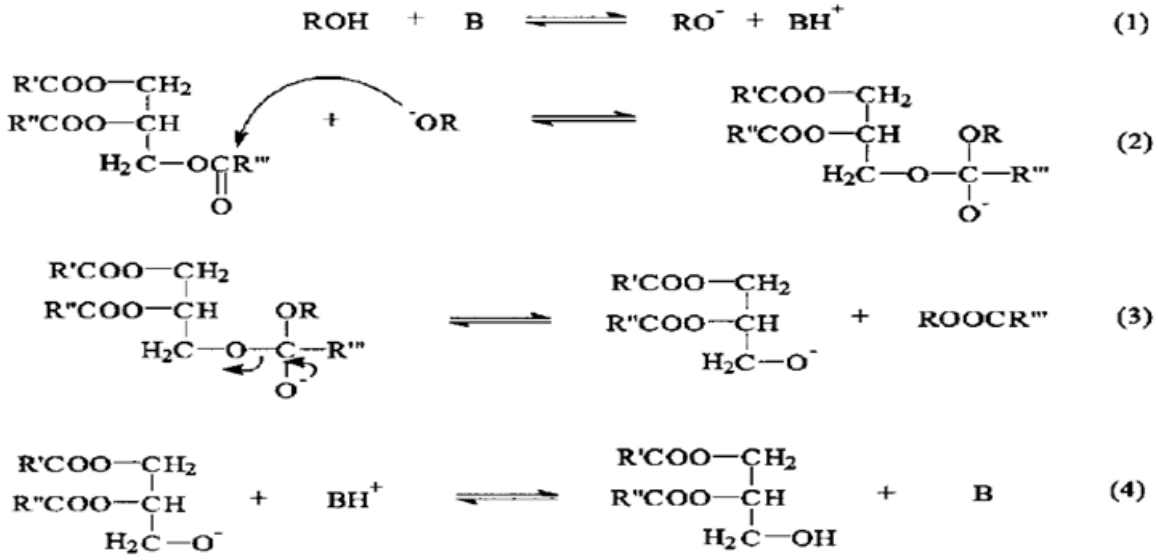

Fig 5. Transesterification mechanism in the presence of water using CaO as catalyst.

6.2. CaOZnO Catalyst

The combination of Cao and ZnO (CaOZnO) catalyst in palm kernel oil **transesterification is studied**. The mixture of CaO and ZnO has small particle size which result in large surface contact area as compared to individual oxides. Ngamcharussrivchai [53] used CaOZnO catalyst with Ca/Zn ratio 0.25 for the transesterification of palm kernel oil and obtained greater than 94% yield at reaction temperature 60°C, methanol to oil ratio 30 and reaction time 60 minute. CaOZnO catalyst is used for the transesterification of sun flower seed oil and 90% yield is obtained [65]. The CaO and ZnO are synthesized by Co-precipitation method or impregnation method. Ngamcharussrivchai [53] found that the catalyst synthesized by the co precipitation method result in higher yield (94.2%) compared to impregnation method (90%). The literature shows that the activity of reaction depends on Ca to Zn atomic ratio it is synthesized between ratio, from ¼ to 4. At atomic ratio of 0.25 the CaOZnO catalyst produce 93.5% of esters which is larger as compared to other atomic ratio.

7. Enzyme catalyzed Transesterification

The problem related to conventional catalytic process, like removal of catalyst treat large amount of waste waterand high energy requirement are solved by using enzymes. Enzyme do not form any soap like alkaline catalyst and without the need of washing they esterify both FFA and TAG in single step. These are biological catalyst and can catalyze different chemical reactions. They can be either used in free or immobilized form in transesterification that leads to the production of biodiesel [66]. A wide range of enzymes such as lipase has been used for esterification [67]. Lipase from fungi and bacteria are mostly used for process and they belong to group of hydrolytic enzymes which is also known as hydrolases.

The lipase catalyzed reaction is classified as [68].
1. hydrolysis 2. Synthesis a) esterification b) transesterification.

1) Hydrolysis

$$R^1COOR^2 + H_2O \rightleftharpoons R^1COOH + R^2OH$$

Esterication

$$R^1COOH + R^2OH \rightleftharpoons R^1COOR^2 + H_2O$$

Transesterification
Alcoholysis

$R^1COOR^2 \rightleftharpoons R^3OH$
$R^1COOR^3 + R^2OH$

Acidolysis

$R^1COOR^2 \rightleftharpoons R^3COOH$
$R^3COOR^2 + R^1COOH$

7.1. Immobilization of Lipase

Immobilization of lipase is the state of arrest of the enzyme in region [69]. Immobilization provide number of benefits such as enzyme reuse, easy separation of product from enzyme [70]. Many other properties are also improved such as chemical, thermal and mechanical properties making them to use in harsher environmental condition [71,72].Salah [73]obtained 25% conversion with immobilized lipase and 3% conversion with free lipase while butanolysis of acetic acid. General technique used for immobilization are 1). Adsorption 2) Entrapment 3) Cross linking 4) Encapsulation . Adsorption is simplest method; in this enzymes are attached to the surface by combination of Vander wall or electrostatic forces.

7.2. Effect Of Presence And Absence Of Solvent Enzyme Based Transesterification

Using enzyme as catalyst for biodiesel production of oil is tried in the presence and absence of solvent. Nelson [74]done methanolysis of tallow oil using hexane as solvent in the presence of Mucormehei lipase and obtained 77.8% yield. But many workers favours solvent free reactions. Furthermore toxicity and inflammability of solvents, prevent the use of solvent enzyme based transesterification. Oznur [76] done transesterification of cotton seed oil using immobilized lipase and obtained 92% of yield in a solvent free medium.

8. Conclusion

This review includes the transesterification of oil using alkali and acid catalyst. The effect of parameters such as, molar ratio, catalyst concentration and methanol to oil ratio are discussed. Selection of homogeneous, heterogeneous and enzymatic catalyst is explained. Homogeneous base catalysts are commonly used for industrial purposes whereas heterogeneous and homogeneous acid catalysts have lesser use. Homogeneous acid and base catalyst require excess alcohol. Homogeneous catalyst is mainly used for batch mode process, followed by catalyst separation. Moreover homogeneous alkali catalysts are sensitive to free fatty acids and H_2O, results in saponification. The feed stock having FFA require acid and base catalyst which is two stage process in which acid catalyst are firstly used and then removed before the use of alkaline catalyst. However the use of acid catalyst increases the corrosiveness. Now a days much more attention is focused on enzyme based catalyst instead of chemical catalyst because enzyme based catalytic reaction proceed at moderate conditions, require low alcohol to oil ratio, and easy product recovery. Use of nano- particle catalyst and heating reactions with the help of microwave is discussed.

9. REFERENCES

[1] Perkins LA, Peterson CL, Durability testing of transesterified winter rape oil (Brassica napus L.) as fuel in small bore, multi-cylinder, DI, CI engines, Society of Automotive Engineers, Warrendale (1991).
[2] Scholl KW, Sorenson SC, Combustion of Soybean oil methyl ester in a direct injection diesel engine, Society of Automotive Engineers, Warrendale (1993).
[3] Zhang Q, Feldman M, Peterson C, Diesel engine durability when fueled with methyl ester of winter Rapeseed oil, American Society of Agricultural Engineers, Washington DC (1988).
[4] Atabani AE, Silitonga AS, Badruddina Irfan Anjum, Mahliaa TMI, Masjukia HH, Mekhilefd S, A comprehensive review on biodiesel as an alternative energy resource andits characteristics, Renewable and Sustainable Energy Reviews, 16, 2070– 2093 (2012).

[7] Demirbas AH, Demirbas I, Importance of rural bioenergy for developing countries, Energy Convers Manage, 48(8):2386–98, (2007).
[8] Fukuda H, Kondo A, Noda H, Biodiesel fuel production by transesterification of oils, J Biosci Bioeng, 92(5):405–16 (2001).
[9] Meher LC, Sagar D Vidya, Naik SN, Technical aspects of biodiesel production by transesterification - a review, Renewable and Sustainable Energy Reviews, xx (xxxx) 1-21 (2004).
[10] Awolu Olugbenga Olufemi and Layokun Stephen Kolawole, Optimization of two-step transesterification production of biodiesel from neem (Azadirachta indica) oil,International Journal of Energy and Environmental Engineering, 4:39 (2013).
[11] Gaurav Kumar, Srivastava Richa and Singh Ram, Exploring biodiesel: chemistry, biochemistry and microalgal source, International journal of green energy, 10: 1-22 (2013).
[12] Meher LC, Sagar D Vidya, Naik SN, Renew. Sustain. Energy Rev., 10, 248–268 (2006).
[13] Kaeida M, Samukawa T, Ban K, Kondo A, Shimada Y, Noda H, Nomoto F, Othsuka K, Yzumoto E, Fukuda H, J. Biosci. Bioeng., 88, 627-631 (1999).
[14] Antolin G, Tinaut FV, Briceno Y, Perez C, Ramirez Al, Biores. Technol., 83, 111-114 (2002).
[15] Srivastava A, Prasad R, Renewable Sustainable Energy Rev., 4, 111-133 (2000).
[16] Zhang Y, Dube MA, Mclean DD, Kates M, Bioresour. Technol., 89, 1–16 (2003).
[17] Freedman B, Pryde EH, Mounts TL, J. Am. Oil Chem. Soc., 61, 1638 (1984).
[18] Sharma YC, Singh B, Fuel, doi:10.1016/j.fuel.2007.08.001 (2007).
[19] Taft RW, Newman MS and Verhoek FH, J Am Chem Soc., 72, 4511 (1947).
[20] Guthrie JP, J Am Chem Soc., 113, 3941 (1991).
[21] Prafulla D and Deng PS, Optimization of biodiesel production from edible and non-edible vegetable oils, Fuel 88:1302–6 (2009).
[22] Sultana Shazia, Khalid Aneela, Ahmad Mushtaq, Zuhairi Ahmad Abdullah, Teong Lee Keat, Zafar Muhammad, and Hassan Fayyaz ul, The production, optimization, and characterization of biodiesel from a novel source: Sinapis alba L., International Journal of Green Energy, 11: 280–291 (2014).
[23] Encinar J M, Gonzalez J F, Rodriguez J J and Tejedor A, Energy Fuels, 16, 443-450 (2002).
[24] Lu J, Deng L, Zhao R, Zhang R, Wang F, Tan T, Pretreatment of immobilized Candida sp. 99–125 lipase to improve its methanol tolerance for biodiesel production, J Mol Catal B: Enzym, 62(1): 5–18 (2010)
[25] Bousquet-Dubouch MP, Graber M, Sousa N, Lamare S, Legoy MD, Alcoholysis catalyzed by Candida antarctica lipase B in a gas/solid system obeys a Ping Pong Bi Bi mechanism with competitive inhibition by the alcohol substrate and water, Biochim Biophys Acta Protein Struct Mol Enzymol, 1550(1): 90–99 (2001).
[26] Li L, Du W, Liu D, Wang L, Li Z, Lipase-catalyzed transesterification of rapeseed oils for biodiesel production with a novel organic solvent as the reaction medium, J Mol Catal B: Enzym, 43(1–4):58–62 (2006).
[27] Ma F, Clements L D, Hanna MA, Trans. Am. Soc. Agr. Eng., 41, 1261 (1998).
[28] Sivasamy Arumugam, Cheah Kien Yoo, Fornasiero Paolo, Kemausuor Francis, Zinoviev Sergey, and Miertus Stanislav, Catalytic applications in the production of biodiesel from vegetable oils, ChemSusChem, 2, 278 – 300 (2009).
[29] Arzamendi G, Arguinarena E, Campo I, Zabala S, Gandia L M, Catal. Today, 133–135, 305 (2008).
[30] Rashid U, Anwar F, Moser B R, Ashraf S, Biomass Bioenergy, 32, 1202 (2008).
[31] Gryglewicz S, Bioresour. Technol., 70, 249 (1999).
[32] Freedman B, Butterfield RO, Pryde EH, J. Am. Oil Chem. Soc., 63, 1375 (1986).
[33] Graille J, Lozano P, Pioch D and Geneste P, Oleagineux, 41, 457-464 (1986).
[34] Ejikeme P M, Waste vegetable oils as alternative to diesel fuel in compression ignition engines, Book of Proceedings, International Workshop on Renewable Energy for Sustainable Development in Africa, NCERD, UNN (2007).
[35] Ejikeme PM, Egbuonu CAC and Anyaogu ID, Fatty Acid Methyl Esters of Melon Seed Oil, Characterization for Potential Fuel Applications, Book of Proceedings, Coalcity Chem, Enugu-Nigeria (2008),
[36] Singh AP, He BB, Thompson JC, Gerpen JH Van, Appl. Eng. Agr., 22, 597 (2006).
[37] Zullaikah S, Lai CC, Vali SR, Ju YH, Bioresour. Technol., 96, 1889 (2005).
[38] Lee Adam F, Bennett James A, Manayil Jinesh C and Wilson Karen, Heterogeneous catalysis for sustainable biodiesel production via esterification and transesterification, Chem. Soc. Rev., 43, 7887 (2014).
[39] Hattori H, Chem. Rev., 95, 537–558 (1995).
[40] Peterson GR and Scarrah WP, J. Am. Oil Chem. Soc., 61, 1593–1597 (1984).
[41] Verziu M, Coman SM, Richards R and Parvulescu VI, Catal. Today, 167, 64–70 (2011).
[42] MacLeod CS, Harvey AP, Lee AF and Wilson K, Chem. Eng. J., 135, 63–70 (2008).
[43] Montero J, Wilson K and Lee A, Top. Catal., 53, 737–745 (2010).
[44] Watkins RS, Lee AF and Wilson K, Green Chem., 6, 335–340 (2004).
[45] Martyanov IN, Sayari A, Appl. Catal. A: Gen., 339, 45 (2008).
[46] Woodford JJ, Parlett CMA, Dacquin JP, Cibin G, Dent A, Montero J, Wilson K and Lee AF, J. Chem. Technol. Biotechnol., 89, 73–80 (2014).
[47] Shu Q, Yang B, Yuan H, Qing S, Zhu G, Catal. Commun., 8, 2159 (2007).
[48] Lotero E, Liu Y, Lopez DE, Suwannakarn K, Bruce DA and Goodwin JG, Ind. Eng. Chem. Res., 44, 5353–5363 (2005).
[49] Dacquin JP, Lee AF and Wilson K, Thermochemical Conversion of Biomass to Liquid Fuels and Chemicals, The Royal Society of Chemistry, 416–434 (2010).
[50] Carrero A, Vicente G, Rodrıguez R, Linares M and Peso GL del, Catal. Today, 167, 148–153 (2011).
[51] Koh TS, Chung KH, J. Kor. Ind. Eng. Chem., 19, 214 (2008).
[52] Kozhevnikov IV, Chem. Rev., 98, 171–198 (1998).
[53] Ngamcharussrivichai C, Totarat P, Bunyakiat K, K, Ca and Zn mixed oxide as a heterogeneous base catalyst for transesterification of palm kernel oil," Appl Catal A, vol. 366, pp. 154-159 (2009).
[54] Cao F, Chen Y, Zhai F, Li J, Wang J, Wang X, Wang S, Zhu W, Biotechnol. Bioeng., 101, 93 (2008).
[55] Lidstrom P, Tierney J, Wathey B, Westman J, Microwave assisted organic synthesis- a review, Tetrahedron, vol. 57, pp. 9225

[56] Patil PD, Gude VG, Mannarswamy A, Cooke P, Munson-McGee S, Nirmalakhandan N, Lammers P, Deng S, Optimization of microwave-assisted transesterification of dry algal biomass using response surface methodology, Bioresource Technology, vol. 102, no. 2, no. 1399-1405 (2011).
[57] Ma L, Chen WX, Zhao J, Zheng YF, Synthesis of Pr(OH)3 and Pr6O11 nanorods by microwave-assisted method: Effects of concentration of alkali and microwave heating time, Journal of Crystal Growth, vol. 303, pp. 590–596 (2007).
[58] Yan S, Kim M, Salley SO, Ng KYS, Oil transesterification over calcium oxides modified with lanthanum, Appl Catal A Gen, 360:163–70 (2009).
[59] Wang J, Chen Y, Wang X, Cao F, Aluminumdodecatungstophosphate (AL0. 9H0.3PW$_{12}$O$_{40}$) nanotube as a solid acid catalyst one-pot production of biodiesel from waste cooking oil, BioResources, 4:1477–86 (2009).
[60] Tanabe K, Yoshii N, Hattori H, Catalytic activity and selectivity of evacuated calcium oxide for isomerization of but-1-ene, J. Chem. Soc D: Chem. Commun., Issue 9, p. 464 (1971).
[61] Liu X, He H, Wang Y, Zhu S, Piao X, Transesterification of soybean oil to biodiesel using CaO as a solid base catalyst, Fuel, vol 87, pp. 216-221 (2008).
[62] Huaping Z, Zongbin W, Yuanxiong C, Ping Z, Shijie D, and Xiaohua L, Preparation of biodiesel catalyzed by solid super base of Calcium Oxide and its refining process, Chin J. Catal., 27: 391-396 (2006).
[63] Serio Di, Ledda M, Cozzolino M, Minutillo G, Tesser R, and Santacesaria E, Transesterification of Soybean Oil to Biodiesel by using Heterogeneous Basic Catalysts, Industrial and Engineering Chemistry Research, 45: 3009-3014 (2006).
[64] Dossin TF, Reyniers MF, Berger RJ, and Marin GB, Simulation of heterogeneously MgO-catalyzed transesterification for fine-chemical and biodiesel industrial production, Appl. Catal. B: Gen, 67:136–148 (2006).
[65] Rubio Alba AC, Gonzalez Santamaria J, Josefa M, Heterogeneous transesterification processes by using CaO supported on Zinc Oxide as basic catalysts, Catalysis Today, 149: 281-287 (2010).
[66] Haas MJ, McAloon AJ, Yee WC, Foglia TA, A process model to estimate biodiesel production costs, Bioresour Technol, 97:671–678 (2006).
[67] Fjerbaek Lene, Christensen Knud V, Norddahl Birgir, A review of the current state of biodiesel production using enzymatic transesterification, Biotechnology and Bioengineering, Vol. 102, No. 5, (2009).
[68] Vulfson EN, In lipases – their structure, biochemistry & application, Woolley P & Petersen SB, eds., 271-288, Cambridge univ. press, Cambridge (1994).
[69] Jegannathan KR, Abang S, Poncelet D, Chan ES and Ravindra P, Production of biodiesel using immobilized lipase-A critical review, Crit. Rev. Biotechnol., 28: 253-264. DOI:10.1080/07388550802428392 (2008)
[70] Peilow AD and Misbah MMA, Immobilization of lipase enzymes and their application in the interesterification of oils and fats, 1st Edn., In: Methods in Biotechnology, Vol.15: Enzymes in Nonaqueous Solvents: Methods and Protocols. Vulfson EN, PJ Halling and HL Holland (Eds). Humana Press Inc., Totowa, New Jersey, ISBN: 089639293, pp: 627-649 (2001).
[71] Awang R, Ghazuli MR, and Basri M, Immobilization of lipase from Candida rugosa on palm-based polyurethane foam as a support material, Am. J. Biochem. Biotechnol., 3: 163-166. ISSN: 1553-3468 (2007).
[72] Bhushan I, Parshad R, Gazi G and Gupta VK, Immobilization of lipase by entrapment in caalginate beads, J. Bioact. Compatible Polym., 23: 552-562 (2008).
[73] Salah RB, Ghamghui H, Miled N, Mejdoub H and Gargouri Y, Production of butyl acetate ester by lipase from novel strain of Rhizopus oryzae, J. Biosci. Bioeng., 103: 368-373 (2007).
[74] Nelson LA, Foglia A & Marman WN, J Am Oil Chem Soc, 73, 1191-1195 (1996).
[75] Hsiao MC, Lin CC, Chang YH, Microwave irradiation assisted transesterification of soybean oil to biodiesel catalyzed by nanopowder calcium oxide, Fuel, vol 90, Issues 5, pp.1963-1969 (2011).
[76] Oznur K, Tuter M & Aksoy HA, Bioresour technol, 83, 125-129 (2002).

Performance Evaluation Of Fouled Evaporator Vapour Compression System

Naveen Solanki[1‡], Akhilesh Arora[2], Raj Kumar Singh[3]

[1]Department of Mechanical and Automation Engineering, Maharaja Agrasen Institute of Technology, PSP Area Sector-22, Rohini Delhi-110086,
E-mail: naveensolanki1984@gmail.com

[2]Department of Mechanical Engineering, Delhi Technological University, Shahbad Daulat Pur, Bawana Road, Delhi-110042
E-mail: akhilesharora@dce.ac.in

[3]Department of Mechanical Engineering, Delhi Technological University, Shahbad Daulat Pur, Bawana Road, Delhi-110042
E-mail: rajkumarsingh@dce.ac.in

[2] Corresponding Author; Tel: 9310279932, Fax: NIL

ABSTRACT

In this paper, effect of evaporator fouling is measured on the performance of a vapour compression system with refrigerants HFO1234yf as a substitute to HFC134a. The condenser coolant temperature ($T_{in,cond}$) has been varied between 35 - 40^{0}C to evaluate the effect of fouling, while keeping the evaporator air inlet temperature ($T_{in,\ evap}$) and efficiency of compressor ($\eta_{cp.ism}$) constant. The conductance of evaporator has been reduced up to 50% for analyzing the effect of fouling on the system performance. A simulation program is developed in Engineering Equation Solver (EES) for computing the results. The fouling decreases the compressor power, cooling capacity and COP. The second law efficiency is also observed to decrease with decrease in the evaporator conductance.

Keywords- Vapour Compression; Compressor; Evaporator; Fouling; R1234yf; R134a

1. INTRODUCTION

Refrigeration involves heat transfer from a low-temperature region to a high-temperature region. This process is typically utilized by means of a Vapour compression refrigeration cycle (VCRC) involving a particular refrigerant. In recent past the most commonly used refrigerants are R11, R12, R500, R22 and R123, but due to their high ODP these refrigerants have either been phased out or are to be phased out in near future. In recent years, HFC134a is used in many refrigeration applications viz. automobile air-conditioning, refrigerators. HFC134a has high GWP, and hence needs replacement by a low GWP refrigerant.

Calm [1] reported HFO1234yf is a low GWP refrigerant. Ding [2] and Cabello et al. [3] have modeled the system components and computed the performance of the vapour compression system. Lee and Jung [4] worked on mobile air-conditioning bench tester under summer and winter conditioning for HFO1234yf and HFC134a. And their results showed that the COP, cooling capacity and discharge temperature (Compressor) for HFO1234yf are 2.7%, 4.0%, and 6.5°C lower as compared to HFC134a. Jarall [5] compared the performance of HFO1234yf with HFC134a at nominal output power (550W) in a refrigeration plant. Their results showed that HFO1234yf gives less cooling capacity, COP, and compressor efficiency by 3.4-13.7%, 0.35-11.88% and 0-6.3% in comparison to HFC134a. Reasor et al. [6] studied that due to environmental concerns, refrigerants with a low global warming impact are gaining importance in the refrigeration industry. Refrigerant R1234yf has a low GWP of 4, compared to 1430 for R134a, and has thermodynamic properties similar to R134a, making it a desirable choice for future automotive refrigerants.

The literature survey shows that HFOs are next generation refrigerants. These are the alternative refrigerants but their performance evaluation is must, before putting them into commercial use. Their performance should be evaluated under ideal and actual working conditions.

During the operation of system, the performance under actual working condition is dependent on the fouling of heat exchanger. The scale deposition on the surfaces of heat exchanger (evaporator) tubes increases thermal resistance and hence affecting the system performance. The sensitivity of the heat exchanger to fouling is

strongly dependent on the type of fouling as well as the specifics of the heat exchanger geometry. Ahn et al. [7] examined experimentally the air-side particulate fouling in fin-and-tube heat exchangers of air conditioners. They observed that the important parameters influencing the fouling of heat exchangers are the concentration and size of indoor pollutants, the filter efficiency, hydrophilicity of fin surfaces and fin spacing. The pressure drop of heat exchangers increases due to the deposition of indoor pollutants larger than 1 μm in size and increases up to 44% in the samples used for 7 years. The air-side particulate fouling degrades the cooling capacity by 10-15% in the samples. Yang et al. [8] discussed the impact of evaporator fouling on the performance of R22 packaged air conditioners. In this study it was found that the equipment cooling capacity is reduced with fouling primarily because of a decrease in airflow due to the increased pressure drop. Fouling affects evaporator-side fan power which in turn affects the equipment EER (Energy Efficiency Ratio) significantly. Comparing the fan power for fouled conditions to the fan power for clean conditions, the variation ranged from approximately –7% to a value as high as 40%.

From the literature survey it clear that there does not exist any study on the effect of fouling when using low GWP HFO refrigerants. Accordingly in this paper the system performance is computed on the basis of combined first law (Energy analysis) and the second law (Exergy analysis) of thermodynamics under fouled conditions for HFO1234yf and HFC134a. The effect of variation in evaporator conductance and condenser coolant inlet temperatures has been examined on the performance of the system. The parameters computed are COP, cooling capacity, compressor work and second law efficiency.

2. MODEL DESCRIPTIONS

The schematic and T-S diagrams of vapour compression system/cycle are shown in figures 1 and 2 respectively.

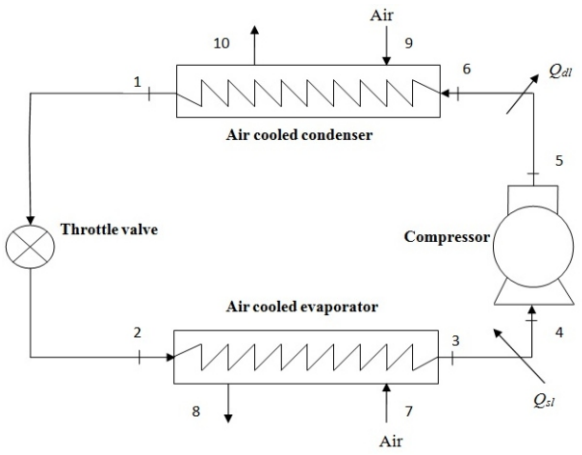

Figure 1: Schematic diagram of a simple VCRS

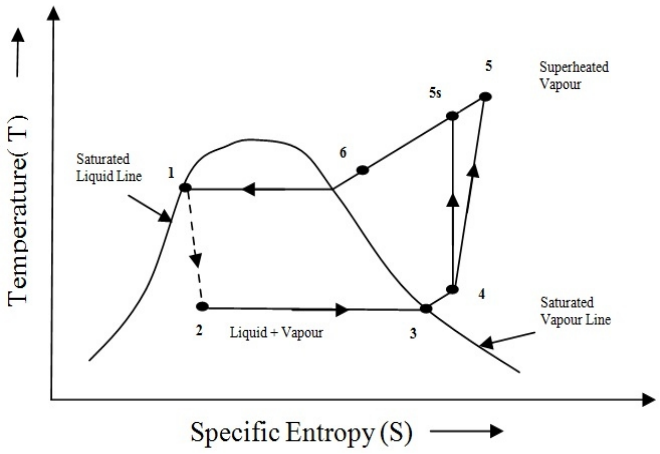

Figure 2: Temperature – Entropy diagram of VCRC

The various processes occurring in vapour compression cycle

i) Process 4-5s: Isentropic compression of the vapour from state 4 to 5s. However the compression is never isentropic and hence in actual compression process (4-5) the exit state from the compressor is 5.

ii) Process 5-6: Heat rejection at constant pressure to the surrounding from the discharge line.

iii) Process 6-1: Heat rejection in condenser at constant pressure.

iv) Process 1-2: An irreversible adiabatic expansion of vapour through the expansion valve or throttling device. The pressure and temperature of the liquid are reduced. The process is accompanied by partial evaporation of some liquid. The process is shown by dotted line because it is irreversible.

v) Process 2-3: Heat absorption in evaporator at constant pressure. The final state 3 the refrigerant is in the dry saturated state at the exit from the evaporator.

vi) Process 3-4: The temperature at the exit is lower than the ambient temperature hence heat is transferred from surroundings to the refrigerant in the suction line at constant pressure.

Considering the steady-state cyclic operation and applying the first law of thermodynamics to the system as shown in Figure 2, the equation (1) can be obtained as under:

$$\dot{Q}_{cond} + \dot{Q}_{loss,\,cond} - (\dot{Q}_{evap} + \dot{Q}_{loss,\,evap}) - \dot{W}_{cp} = 0 \quad (1)$$

The heat-transfer rate in the evaporator is given by:

$$\dot{Q}_{evap} = \dot{m}_{ref}(h_3 - h_2) \quad (2)$$

In terms of effectiveness (ϵ), minimum heat capacity (C_{min}) and temperature difference $\dot{Q}_{evap}$ can be written as

$$\dot{Q}_{evap} = (\epsilon C_{min})_{evap}(T_7 - T_2) \quad (3)$$

Where T_2 is the temperature of refrigerant entering to evaporator and T_7 is the outside air temperature entering to evaporator.

Similarly, the heat-transfer rate in the condenser is given by

$$\dot{Q}_{cond} = \dot{m}_{ref}(h_6 - h_1) = (\epsilon C_{min})_{cond}(T_1 - T_9) \quad (4)$$

Where T_1 is the temperature of saturated liquid refrigerant leaving the condenser and T_9 is the outside air temperature entering the condenser for cooling the refrigerant in the condenser.

The power required by the compressor is presented in terms of isentropic efficiency of the compressor, given by

$$\dot{W}_{cp} = \dot{m}_{ref}(h_5 - h_4) = \frac{\dot{m}_{ref}(h_{5s} - h_4)}{\eta_{cp,isn}} \quad (5)$$

Where point 5 shows the actual state of refrigerant vapour at the exit from compressor.

Work input to the compressor can also be expressed using steady flow energy equation as under:

$$\dot{Q}_{cp} - \dot{W}_{cp} = \dot{m}_{ref}(h_5 - h_4) \quad (6)$$

Where $\dot{Q}_{cp}$ is the heat transfer from the compressor to the surrounding.

The heat leaking into the suction line is represented by

$$\dot{Q}_{sl} = \dot{m}_{ref}(h_4 - h_3) \quad (7)$$

The heat leakage from the discharge line to surrounding can be expressed as

$$\dot{Q}_{dl} = \dot{m}_{ref}(h_6 - h_5) \quad (8)$$

The COP is the ratio of refrigerating effect to compressor power, i.e.

$$COP = \frac{Q_{evap}}{W_{cp}} \quad (9)$$

The first law efficiency alone is not a realistic measure of performance of engineering device. To overcome this deficiency, we define second-law efficiency (η_{II}) of a refrigeration system which is the ratio of the actual coefficient of performance (COP) to the maximum possible coefficient of performance (COP_{rev}) under the same operating conditions.

$$\eta_{II} = \frac{COP}{COP_{rev}} = \frac{\eta_I}{\eta_{th,rev}} \quad (10)$$

$$\text{Where, } COP_{rev} = \frac{T_7}{T_9 - T_7} \quad (11)$$

The effectiveness of a heat exchanger is defined using equation (12) as under

$$\epsilon = \frac{\text{Actual heat transfer}}{\text{maximum possible heat transfer}} \qquad (12)$$

The effectiveness of evaporator and condenser is given by equation 13 and 14

$$\epsilon_{evap} = \frac{T_7 - T_8}{T_7 - T_2} \qquad (13)$$

$$\epsilon_{cond} = \frac{T_{10} - T_9}{T_6 - T_9} \qquad (14)$$

Incropera et al. [9] derived the expression for relation between effectiveness, heat capacity and overall conductance (UA) which is expressed as

$$UA = C_{min} * ln\left(\frac{1}{1-\epsilon}\right) \qquad (15)$$

The fouling on air side of a heat exchanger is the reason for reduction of UA. The percentage reduction in conductance is represented using the equation (16).

$$UA\% = \left(1 - \frac{UA}{UA_{cl}}\right) * 100 \qquad (16)$$

The above methodology is used to develop a program, for performance computation, in Engineering Equation Solver (EES).

3. RESULTS AND DISCUSSION

The thermodynamic model given above is used to evaluate the performance of vapour compression system. The performance is evaluated with two refrigerants (R134a and R1234yf).

Input conditions

The values given in table 1 are used for computation of results in current work.

Table 1: Values of inputs at design point.

Parameters	Values
Inlet Evaporator coolant temperature ($T_{in,evap} = T_7$ in K)	273
Inlet Condenser coolant temperature ($T_{in,cond} = T_9$ in K)	308-313
Cooling Capacity (Q_{evap} in kW)	100
Product of condenser effectiveness and capacitance rate of external fluid [$(\epsilon C_{min})_{cond}$, kW/K]	9.39
Product of evaporator effectiveness and capacitance rate of external fluid [$(\epsilon C_{min})_{evap}$, kW/K]	8.2
Isentropic efficiency of compressor ( )	0.65
Effectiveness ([a])	0.80
Refrigerants	R134a and R1234yf

Effect of evaporator fouling (evaporator conductance for R134a) on percentage change in compressor power, cooling capacity and COP

Figures 3, 4 and 5 represent the effect of evaporator fouling with variation in condenser coolant temperature for the refrigerants R134a and R1234yf respectively. It is observed that with increase in evaporator fouling the compressor power, cooling capacity and COP decreases.

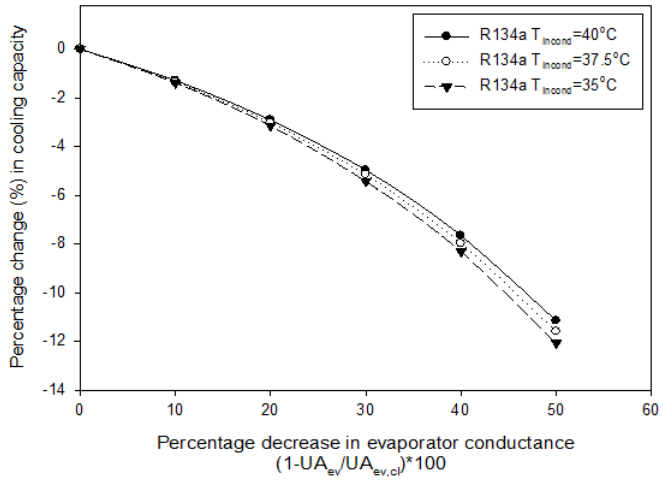

Figure 3: Percentage change in cooling capacity v/s percentage decrease in evaporator conductance for R134a.

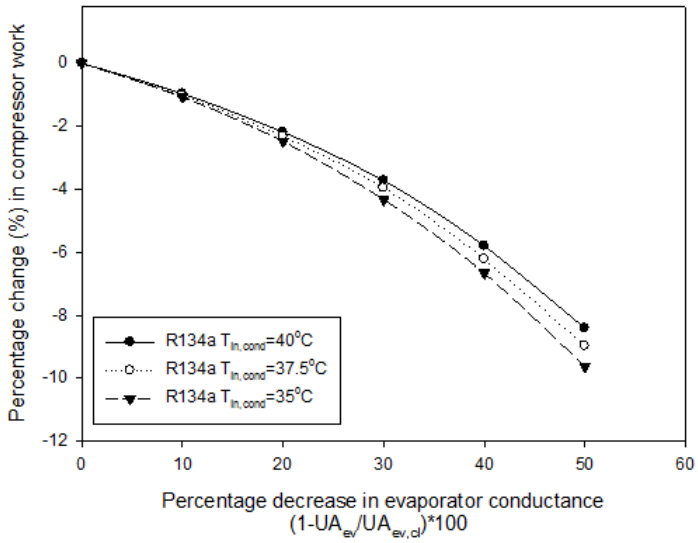

Figure 4: Percentage change in compressor work v/s percentage decrease in evaporator conductance for R134a.

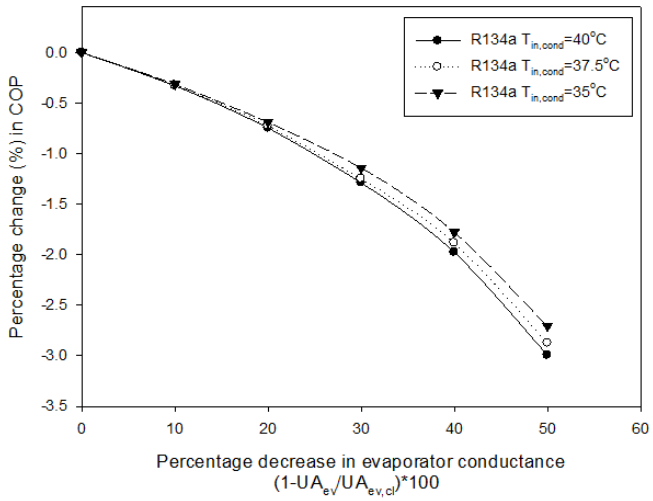

Figure 5: Percentage change in COP v/s percentage decrease in evaporator conductance for R134a.

The effect of evaporator fouling with variation in condenser coolant temperature decreases the COP, because with percentage decrease in evaporator conductance ($(1-UA_{ev}/UA_{ev,cl})*100$), cooling capacity and compressor work both decrease. However the cooling capacity decreases at a higher rate as compared to compressor work.

Figures 6, 7 and 8 show the variation of percentage changes (%) in Q_{evap}, W_{cp}, and COP with percentage decrease in evaporator conductance for R1234yf.

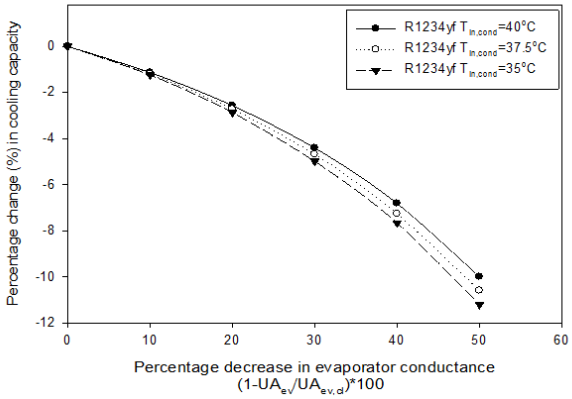

Figure 6: Percentage change in cooling capacity v/s percentage decrease in evaporator conductance for R1234yf.

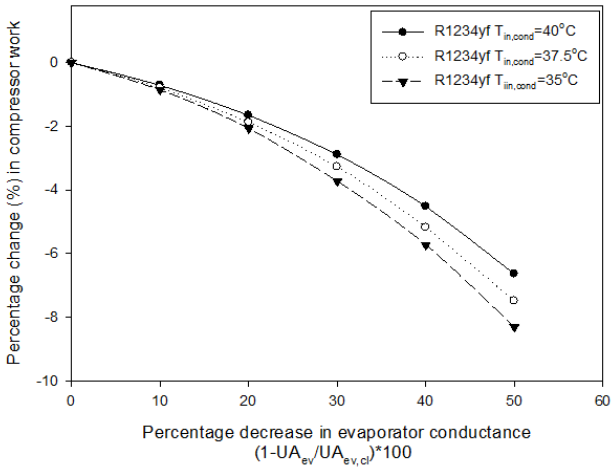

Figure 7: Percentage change in compressor work v/s percentage decrease in evaporator conductance for R1234yf.

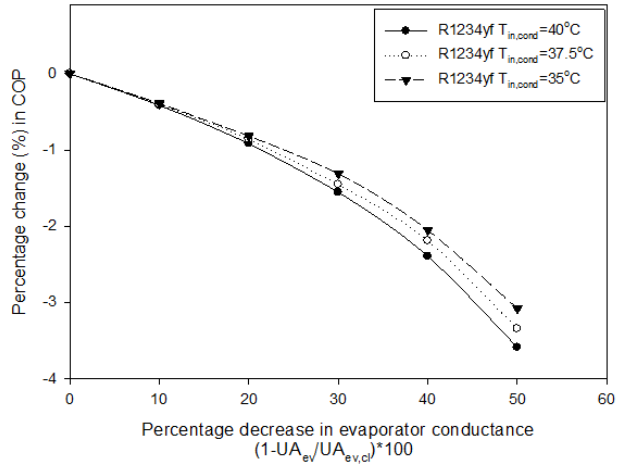

Figure 8: Percentage change in COP v/s percentage decrease in evaporator conductance for R1234yf.

The trends are similar in figures 6 to 8 for R1234yf when compared with the results of R134a shown in figures 3 to 5; hence it does not require explanation. The percentage decrease in the values of cooling capacity and compressor power is more in case of HFC134a as compared to HFO1234yf. However the percentage decrease in COP for HFO1234yf is more than HFC134a. The decrease in value of COP for R1234yf is 3.59% and for R134a is 2.99%.

Figures 9 and 10 show the variation of second-law efficiency (η_{II}) %, with evaporator fouling from 0% to 50%, at $T_{in,cond} = 40^{\circ}C, 37.5^{\circ}C, 35^{\circ}C$, for refrigerants R134a and R1234yf.

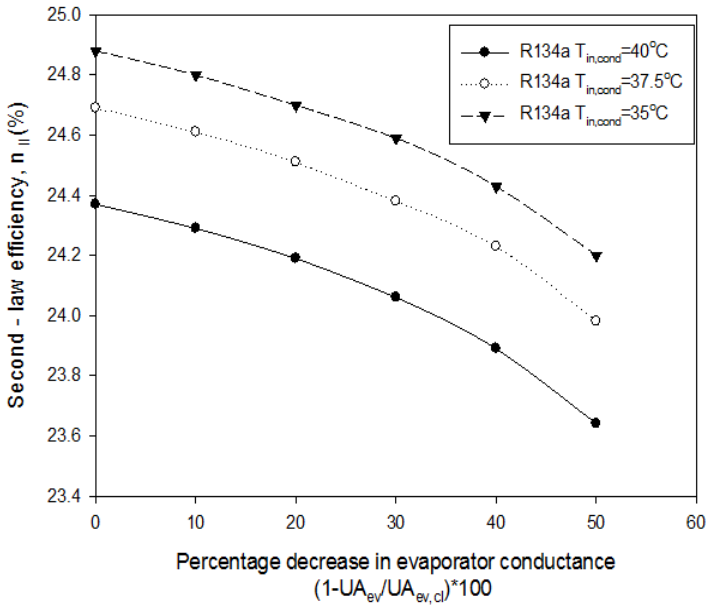

Figure 9: Second-law efficiency (%) v/s percentage decrease in evaporator conductance for R134a.

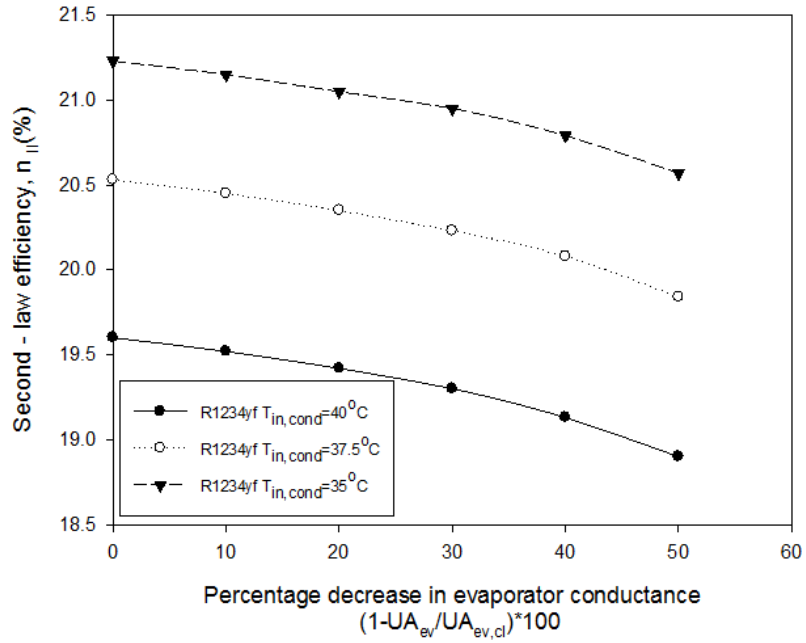

Figure 10: Second-law efficiency (%) v/s percentage decrease in evaporator conductance for R1234yf.

The comparison of the result of second – law efficiency at condenser inlet temperature of 40°C, 37.5°C, & 35°C for unfouled condition & 50% reduction in evaporator conductance due to fouling are shown in Table 2.

Table 2 : Comparison of second-law efficiency (evaporator under fouled condition) for Refrigerant R1234yf with R134a.

Refrige-rant	Change in UA_{evap} (%)	$?_{II}$ (%) $T_{in,cond}$ =40°C	$?_{II}$ (%) $T_{in,cond}$ =37.5°C	$?_{II}$ (%) $T_{in,cond}$ =35°C
R1234yf	0	19.60	20.53	21.23
	50	18.90	19.84	20.57
R134a	0	24.37	24.69	24.88
	50	23.64	23.98	24.20

From the above table it is clear that, the second-law efficiency for R1234yf is about 5-6% lower than R134a under clean as well as fouled condition.

4. CONCLUSIONS

On the basis of results obtained from thermodynamic model, following conclusions are drawn-

Effect of fouling on the performance of a simple vapour compression cycle has been evaluated by varying condenser coolant inlet temperature $T_{in,cond}$ (i.e. 35°C, 37.5 °C and 40 °C), and also by varying evaporator conductances (i.e. 0% - 50%), for the refrigerant R134a and R1234yf.

In evaporator fouling it has been observed that:-

It is observed that the evaporator fouling has larger effect on cooling capacity (evap%) as it decreases by 12.08 for R134a and 11.19 for R1234yf. The compressor power (cp%) also decreases by 9.63 for R134a and 8.31 for R1234yf. The maximum percentage decrease in value of COP for R1234yf and R134a is 3.59 and 2.99 respectively. The second-law efficiency is also observed to decrease with decrease in the evaporator conductance for both Refrigerants (R134a and R1234yf).

5. *REFERENCES*

[1] Calm, J., 2008. The next generation of refrigerants – Historical review, considerations, and outlook. International Journal of Refrigeration 31: 1123-1133.

[2] Ding, G., 2007. Recent development in simulation techniques for vapour-compression refrigeration systems. International Journal of Refrigeration 1-15.

[3] Cabello, R., J., Navarro and E., Torrella, 2005. Simplified steady-state modelling of a single stage vapour compression plant Model development and validation. Applied Thermal Engineering 25, 1740–1752.

[4] Lee, Y., and D. Jung, 2011. A brief performance comparison of R1234yf and R134a in a bench tester for automobile application. Applied Thermal Engineering 35: 240-242.

[5] Jarall, S. 2012. Study of refrigeration with HFO-1234yf as a working fluid. International Journal of Refrigeration 35: 1668-1677.

[6] Reasor, P., V., Aute, and R. Radermacher. 2010. Refrigerant R1234yf Performance Comparison Investigation. International Refrigeration and Air Conditioning Conference at Purdue University Paper No.1085.

[7] Ahn, Y., S., Cheong, Y., Jung, and J., Lee, 2006. An Experimental Study of the Air-Side Particulate Fouling in Fin-and-Tube Heat Exchangers of Air Conditioners. International Refrigeration and Air Conditioning conference at Purdue University Paper No. 818..

[8] Yang, L., J., E., Braun, and E., A., Groll, 2004. The Impact of Evaporator Fouling on the Performance of Packaged Air Conditioners. International Refrigeration and Air Conditioning Conference at Purdue University Paper No. 687.

[9] Incropera, F.P., D.P. DeWitt, T., Bergman, and A. Lavine. 2006. Fundamentals of Heat and Mass Transfer. New York: John Wiley & Sons.

NOMENCLATURE

C-	Minimum value of the thermal Capacitance rate (kWK^{-1})
CFCs-	Chloro-fluoro-carbons
COP-	Coefficient of performance
EES-	Engineering equation solver
GWP-	Global warming potential
HCFCs-	Hydro-chloro-fluoro-carbons
HFO-Hydro-	Fluoro-Olefin
m-	Refrigerant mass flow rate ($kg\ s^{-1}$)
υ-	Specific volume (m3 kg-1)
ODP-	Ozone depletion potential
P-	Pressure (MPa)
Q-	Rate of heat transfer (kW)
T-	Temperature (K)
UA-	Overall conductance (kWK^{-1})
VCRC-	Vapour compression refrigeration cycle
VCRS -	Vapour compression refrigeration system
W-	Power requirement (kW)

Greek

Ƞ-	Efficiency (%)
Ɛ-	Heat exchanger effectiveness

Subscripts

Act-	Actual
cl-	Clean condition
cd, cond-	Condenser
ev, evap-	Evaporator
cp-	Compressor
dl-	Discharge line
sl-	Suction line
f-	Fouled condition
isn-	Isentropic

Instructions for Authors

Essentials for Publishing in this Journal

1 Submitted articles should not have been previously published or be currently under consideration for publication elsewhere.

2 Conference papers may only be submitted if the paper has been completely re-written (taken to mean more than 50%) and the author has cleared any necessary permission with the copyright owner if it has been previously copyrighted.

3 All our articles are refereed through a double-blind process.

4 All authors must declare they have read and agreed to the content of the submitted article and must sign a declaration correspond to the originality of the article.

Submission Process

All articles for this journal must be submitted using our online submissions system. http://enrichedpub.com/ . Please use the Submit Your Article link in the Author Service area.

Manuscript Guidelines

The instructions to authors about the article preparation for publication in the Manuscripts are submitted online, through the e-Ur (Electronic editing) system, developed by **Enriched Publications Pvt. Ltd**. The article should contain the abstract with keywords, introduction, body, conclusion, references and the summary in English language (without heading and subheading enumeration). The article length should not exceed 16 pages of A4 paper format.

Title

The title should be informative. It is in both Journal's and author's best interest to use terms suitable. For indexing and word search. If there are no such terms in the title, the author is strongly advised to add a subtitle. The title should be given in English as well. The titles precede the abstract and the summary in an appropriate language.

Letterhead Title

The letterhead title is given at a top of each page for easier identification of article copies in an Electronic form in particular. It contains the author's surname and first name initial .article title, journal title and collation (year, volume, and issue, first and last page). The journal and article titles can be given in a shortened form.

Author's Name

Full name(s) of author(s) should be used. It is advisable to give the middle initial. Names are given in their original form.

Contact Details

The postal address or the e-mail address of the author (usually of the first one if there are more Authors) is given in the footnote at the bottom of the first page.

Type of Articles

Classification of articles is a duty of the editorial staff and is of special importance. Referees and the members of the editorial staff, or section editors, can propose a category, but the editor-in-chief has the sole responsibility for their classification. Journal articles are classified as follows:

Scientific articles:

1. Original scientific paper (giving the previously unpublished results of the author's own research based on management methods).
2. Survey paper (giving an original, detailed and critical view of a research problem or an area to which the author has made a contribution visible through his self-citation);
3. Short or preliminary communication (original management paper of full format but of a smaller extent or of a preliminary character);
4. Scientific critique or forum (discussion on a particular scientific topic, based exclusively on management argumentation) and commentaries. Exceptionally, in particular areas, a scientific paper in the Journal can be in a form of a monograph or a critical edition of scientific data (historical, archival, lexicographic, bibliographic, data survey, etc.) which were unknown or hardly accessible for scientific research.

Professional articles:

1. Professional paper (contribution offering experience useful for improvement of professional practice but not necessarily based on scientific methods);
2. Informative contribution (editorial, commentary, etc.);
3. Review (of a book, software, case study, scientific event, etc.)

Language

The article should be in English. The grammar and style of the article should be of good quality. The systematized text should be without abbreviations (except standard ones). All measurements must be in SI units. The sequence of formulae is denoted in Arabic numerals in parentheses on the right-hand side.

Abstract and Summary

An abstract is a concise informative presentation of the article content for fast and accurate Evaluation of its relevance. It is both in the Editorial Office's and the author's best interest for an abstract to contain terms often used for indexing and article search. The abstract describes the purpose of the study and the methods, outlines the findings and state the conclusions. A 100- to 250-Word abstract should be placed between the title and the keywords with the body text to follow. Besides an abstract are advised to have a summary in English, at the end of the article, after the Reference list. The summary should be structured and long up to 1/10 of the article length (it is more extensive than the abstract).

Keywords

Keywords are terms or phrases showing adequately the article content for indexing and search purposes. They should be allocated heaving in mind widely accepted international sources (index, dictionary or thesaurus), such as the Web of Science keyword list for science in general. The higher their usage frequency is the better. Up to 10 keywords immediately follow the abstract and the summary, in respective languages.

Acknowledgements

The name and the number of the project or programmed within which the article was realized is given in a separate note at the bottom of the first page together with the name of the institution which financially supported the project or programmed.

Tables and Illustrations

All the captions should be in the original language as well as in English, together with the texts in illustrations if possible. Tables are typed in the same style as the text and are denoted by numerals at the top. Photographs and drawings, placed appropriately in the text, should be clear, precise and suitable for reproduction. Drawings should be created in Word or Corel.

Citation in the Text

Citation in the text must be uniform. When citing references in the text, use the reference number set in square brackets from the Reference list at the end of the article.

Footnotes

Footnotes are given at the bottom of the page with the text they refer to. They can contain less relevant details, additional explanations or used sources (e.g. scientific material, manuals). They cannot replace the cited literature.
The article should be accompanied with a cover letter with the information about the author(s): surname, middle initial, first name, and citizen personal number, rank, title, e-mail address, and affiliation address, home address including municipality, phone number in the office and at home (or a mobile phone number). The cover letter should state the type of the article and tell which illustrations are original and which are not.

Address of the Editorial Office:

Enriched Publications Pvt. Ltd.
S-9,IInd FLOOR, MLU POCKET,
MANISH ABHINAV PLAZA-II, ABOVE FEDERAL BANK,
PLOT NO-5, SECTOR -5, DWARKA, NEW DELHI, INDIA-110075,
PHONE: - + (91)-(11)-45525005

Notes: